Forschungszentrum Karlsruhe
Technik und Umwelt

Wissenschaftliche Berichte
FZKA 6341

Model and Experiments Related to Laminar Mixed Convection in Two-dimensional far Wakes above Heated/Cooled Bodies

P. Ehrhard

Institut für Kern- und Energietechnik

Oktober 1999

Forschungszentrum Karlsruhe

Technik und Umwelt

Wissenschaftliche Berichte

FZKA 6341

Model and experiments related to laminar mixed convection in two-dimensional far wakes above heated/cooled bodies

P. Ehrhard

Institut für Kern- und Energietechnik

Forschungszentrum Karlsruhe GmbH, Karlsruhe
1999

Als Manuskript gedruckt

Forschungszentrum Karlsruhe GmbH
Postfach 3640, 76021 Karlsruhe

Mitglied der Hermann von Helmholtz-Gemeinschaft
Deutscher Forschungszentren (HGF)

ISSN 0947-8620

Model and experiments related to laminar mixed convection in two-dimensional far wakes above heated/cooled bodies

In a vertically rising forced flow a heated or cooled body is positioned. This develops both a kinematic and a thermal wake, the latter one stipulates buoyant effects in the otherwise forced flow field. An asymptotic model is developed to treat this mixed convection in both plane and axisymmetric geometry. The model holds for laminar flow in boundary layer approximation and engages in a far-wake expansion for weak buoyant forces. For plane geometry the model is validated against both experiments in water and FEM simulations.

It is found for a heated wake that buoyant forces accelerate the fluid in the thermal wake such that the vertical velocity defizit in the kinematic wake is reduced. This may for strong heating even lead to vertical velocities larger than the forced flow amplitude. In conjunction the entrainment is intensified in a heated wake. The effects in a cooled wake are opposit in that the vertical velocity defizit is increased within the thermal wake and the horizontal flow into the wake is weakened. In a strongly cooled wake the horizontal flow may even be inverted, leading from the wake centre into the ambient. The Prandtl number controles the width of the thermal wake and, thus, the portion of the kinematic wake which is effected by buoyant forces. Large Prandtl numbers result in narrow thermal wakes, small Prandtl numbers give wide thermal wakes.

Modell und Experimente zur laminaren Mischkonvektion im zweidimensionalen Nachlauf über beheizten/gekühlten Körpern

In einer von unten nach oben verlaufenden Zwangsströmung wird ein beheizter oder gekühlter Körper positioniert. Dies bedingt einen kinematischen und einen thermischen Nachlauf, wobei der letztere Auftriebseffekte in die Zwangsströmung einbringt. Ein asymptotisches Modell wird entwickelt, welches diese Mischkonvektion in ebener und achsensymmetrischer Geometrie beschreibt. Das Modell ist für laminare Strömung in Grenzschichtapproximation sowie für den fernen Nachlauf bei schwachem Auftrieb gültig. Für die ebene Geometrie wird eine Validierung anhand von Experimenten in Wasser und anhand von FEM-Simulationen durchgeführt.

Im beheizten Nachlauf beschleunigen die Auftriebskräfte das Fluid in der erwärmten Zone, sodaß sich das Defizit der vertikalen Geschwindigkeit reduziert. Dies kann bei starker Beheizung sogar zu Vertikalgeschwindigkeiten führen, welche größer als die Geschwindigkeit der Anströmung sind. In Verbindung damit wird die horizontale Zuströmung von Fluid in den Nachlauf verstärkt. Die Auswirkung eines gekühlten Körpers ist gerade umgekehrt. Hier führt das kalte Fluid im Nachlauf zu einer Verstärkung des Geschwindigkeitsdefizits und so zu einer schwächeren horizontalen Zuströmung. Für stark gekühlte Körper ist gar eine Strömung aus dem Nachlauf in den Außenbereich möglich. Die Prandtl-Zahl kontrolliert die Breite des thermischen Nachlaufs und somit die Zone in welcher Auftriebskräfte wirksam werden. Große Prandtl-Zahlen bedingen einen schlanken thermischen Nachlauf, kleine Prandtl-Zahlen bedingen einen weiten thermischen Nachlauf.

CONTENTS

1. Introduction

Problems involving the combined effects of forced and natural heat convection typically receive little attention. This seems to be the case because in most practical applications either the forced convection or the natural convection dominates and the secondary effects can be neglected in a first approximation. In many important applications, however, both convective modes play an equally-important role and, thus, have to be considered simultaneously. This article relates to such a problem.

We consider specifically a vertically rising forced flow, which passes in cross-flow a cylindrical (or spherical) body and develops a wake downstream. The body is at high temperature, such that the transfered heat leads to buoyant forces in the wake. This situation is of relevance for a number of engineering applications as e.g. hot-wire anemometry or heat exchangers. The flow is assumed to be laminar, which is true only in a limited range of parameters. Therefore, the prctical relevance may be limited, as in many applications wake flows turn turbulent due to inflection-type velocity profiles. The method of treating this mixed-convection problem, however, should apply likewise to turbulent flows in conjunction with simple (analytical) turbulence models.

We may roughly understand this mixed-convection problem as a superposition of a wake flow and a buoyant plume. The first incredience, thus, is the wake flow. We shall focus onto far laminar wakes. The theoretical treatment of far wakes starts with the work of Tollmien (1931). Based on boundary layer theory he develops a first-order approximation to the asymptotic form of a plane far wake behind a slender body, valid for large distances downstream. Goldstein (1933) proceeds to a second-order approximation to the asymptotic form and, moreover, attemps to derive a third-order approximation. Due to a singular behaviour of the third-order approximation, he rejects this approximation. It is Stewartson (1957), finally, who explains the origin of the difficulty at the third stage of approximation and who resolves the problem by adding an appropriate term. A detailed review and discussion of the stages of approximation is given by Berger (1971). In summary, for the plane far wake an asymptotic solution is available, refined to a third-order expansion. This solution in all stages of approximation gives self-similar velocity profiles far downstream of the body. For the axisymmetric far wake equivalent methods have been applied e.g. by Berger (1968) and an analogous asymptotic solution has been obtained. Again, Berger (1971) reviews the progress and the solution of the axisymmetric problem in full detail.

The second incredience of this mixed convection problem is the buoyant plume. Once more, we concentrate on the laminar flow and temperature field above a line (point) heat source. Plumes generated by free convection are the subject of numerous investigations. Zeldovich (1937) is to our knowledge the first author to theoretically recognize the self-similar form of flow and temperature fields in buoyant plumes. Schuh (1948) in turn presents a complete analysis based on boundary layer theory. He derives the coupled set of differential equations and boundary conditions for the problem. Yih (1952) infers closed-form solutions to this set of equations for the specific Prandtl numbers $Pr = \frac{2}{3}, \frac{7}{3}$. A more complete theoretical treatment of plane laminar plumes is conducted by Fujii (1963). He derives a closed-form solution for $Pr = 2$ and, moreover, uses numerical integration to solve the two point boundary value problem for $Pr = 0.01, 0.7, 10$. Aside of a further exact solution for $Pr = \frac{5}{9}$ by Brand & Lahey (1967), Gebhart et al. (1970) give a systematic review of the theoretical approaches and provide further solutions in the complete range $0.01 \leq Pr \leq 100$, obtained by numerical integration. A recent numerical, fully nonlinear treatment of the plane laminar problem is conducted by Liñán & Kurdyumov (1998). Further, asymptotic methods are

engaged to develop solutions for the limiting cases of small and large Prandtl numbers by e.g. Spalding & Cruddace (1961) or Kuiken & Rotem (1971). The above list of theoretical studies by far is not complete, but an extensive review can be found in the book of Gebhart et al. (1988). There are likewise experimental investigations of the problem in literature. The work of Rouse et al. (1952) e.g. relates to a plane plume, rising above a line of small gas flames. Further examples are the experiments of Brodowicz & Kierkus (1966) or Forstrom & Sparrow (1967), where precise flow and temperature fields are measured above heated wires in air. Again, a complete review of the experimental investigations can be found in Gebhart et al. (1988). To summarize, the problem of a plane, laminar plume above a line heat source can be treated within the framework of boundary layer theory and self-similar solutions are obtained. The theoretical and experimental treatment of axisymmetric, laminar plumes has been developed to an equivalent stage, as discussed theoretically e.g. by Schuh (1948), Yih (1951), Fujii (1963), Brand & Lahey (1967), Crane (1975), experimentally e.g. by Rouse et al. (1952) and reviewed by Gebhart et al. (1988).

The combined occurance of both phenomena, namely forced and natural convection behind a heated cylindrical or spherical body, has also been studied in the past. In a first class of theoretical investigations the body is idealized as a line or point heat source, positioned in an otherwise undisturbed, parallel flow. Thus, the presence of the body of finite size is ignored kinematically and only buoyant forces due to the introduced heat are present. Based on boundary layer theory Afzal (1981) develops two expansions, valid for weak/strong buoyant forces in the near/far-field of a line heat source. The forced flow is upward or downward in the gravitational field, such that buoyant forces are favourable or adverse with respect to the forced flow. The corresponding axisymmetric problem of mixed convection behind a point heat source is theoretically treated by Riley & Drake (1983), Afzal (1983) and Afzal (1985). All authors invoke boundary layer theory and infer solutions by means of asymptotic methods. Riley & Drake (1983) develop two solutions for weak/strong buoyant forces, uniformly valid downstream of the heat source in the entire region. Similarly, in the study of Afzal (1983) two expansions for weak/strong buoyant forces in conjunction with a spatial change over are obtained. Finally, Afzal (1985) presents a new formulation, capturing both the weakly- and the strongly-buoyant regime in a single set of equations. Wesseling (1975), in contrast to the above authors, avoids boundary layer approximation and uses instead the Oseen-Boussinesq equations as basis of his analysis. He develops asymptotic solutions for weak buoyant forces, which enable to access the field variables in the near field of the (line) point heat source.

The second class of theoretical investigations consideres the finite size of the body to some extend. Here, the deflection of the flow around the body, the no-slip condition and some thermal condition on the body contour arise. Wood (1972) develops a three-zone model for the plane mixed convection around a heated cylinder. He consideres (i) an inner, diffusive zone immediately around the cylinder, (ii) a wake zone downstream of the cylinder and (iii) an outer zone with irrotational flow and works out the dominant physics and coupling of these zones. The corresponding axisymmetric problem, i.e. mixed convection from a sphere, is treated by Hieber & Gebhart (1969).

There are likewise some experimental investigations of mixed convection from cylinders (wires) in the literature. Collis & Williams (1959) or Hatton et al. (1970) are just a few examples. A more complete review of the experimental work can be found in Gebhart & Pera (1970). In summary, experiments cover a range of Prandtl numbers $0.7 \leq Pr \leq 63$ (air, silicone oils) and focus mostly onto the integral heat transfer from

the cylinder. Measurements of field variables around the body and downstream in the wake are not available to our knowledge.

The present article concentrates on the wake of a heated cylindrical (spherical) body in some distance downstream of its position. This follows to some extend the idea of Wood (1972), particularly with respect to the 'wake zone'. Based on boundary layer theory, we shall develop an asymptotic model by means of a two-parameter expansion. The small parameters are (i) an inverse power of the downstream coordinate and (ii) the ratio of buoyancy and inertia forces. Thus, the model holds far downstream for weakly-buoyant conditions. For such a model the details of the flow and temperature fields around the body are not really relevant. Instead, an integral representation of the effects of the body is sufficient. Firstly, the loss of momentum in the flow is introduced via the drag coefficient of the body. With respect to the pure wake, the model is of second order, in accordance with the expansions of Goldstein (1933) and Berger (1968). Secondly, an intregral amount of heat is introduced at the position of the body. Here the present model is in accord with Wood (1972) as far as the plane formulation is concerned. With respect to Wood (1972) the difference lies in the presence of second-order, nonlinear terms, which allow for a more accurate description of the wake. The present axisymmetric formulation should occur for the first time in literature.

The results from the asymptotic models are worked out with respect to both flow and temperature fields for realistic values of the parameters. This goes far beyond the intention of Wood (1972). Detailed experiments in water, capturing all field variables downstream of a cylinder are further employed to verify the results from the asymptotic model. Such experiments are to our knowledge not yet present in the literature. Numerical (FEM) simulations of the full plane problem serve as a further means to elucidate possible deficiencies of the approximations.

2. Formulation

2.1. *Description of the problem*

Let us consider a cylindrical or spherical body in a parallel flow of speed w_∞ and temperature T_∞ as sketched in figure 1. The flow is upward against the gravitational field. In addition through a constant body temperature $T_b > T_\infty$ an integral heat flux $\dot{Q}$ (respectively a heat flux per unit length $\dot{q}$ for the plane problem) is added to the flow. Firstly, due to the pure presence of the body of diameter d the flow will be deflected as it passes the body. At very low w_∞ the flow will be attached around the complete body. If w_∞ is increased the flow will form a steady recirculating zone behind the body extending a few diameters d downstream. Further downstream streamlines of both sides reapproach each other. At even larger w_∞ the flow will be time-dependent and an oscillatory wake will be observed. We shall restrict the analysis to the steady regime, i.e. to laminar and steady wakes. The second effect of the body is due to the no-slip condition on the body contour, resulting in an integral loss of momentum. Consequently a drag force F_z (respectively a drag force per unit length f_z for the plane problem) applies to the body and reduced velocity amplitudes are a characteristic of the downstream wake. Up to this point we have no buoyant effects involved. If we heat the body, thirdly, we will have hot fluid in the wake. Due to a reduced density of the heated fluid, buoyant forces will tend to accelerate the fluid in the wake. Thus, a faster fill up of the wake, or velocity amplitudes even above w_∞ will be the consequence.

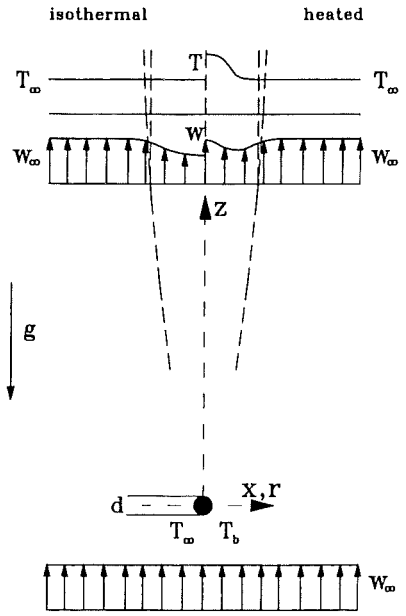

FIGURE 1. Sketch of the problem given for both an isothermal body and a heated body

2.2. *Basic equations and scaling*

If we consider a Newtonian fluid and invoke the Boussinesq approximation, the steady velocity and temperature fields in the fluid are governed by the Navier-Stokes, the continuity and the heat transport equations. Thus, we have

$$\rho_\infty(\boldsymbol{v}\cdot\boldsymbol{\nabla})\boldsymbol{v} = -\boldsymbol{\nabla}p + \mu\boldsymbol{\nabla}^2\boldsymbol{v} + \alpha g\rho_\infty(T - T_\infty)\boldsymbol{e}_z, \tag{2.1}$$

$$\boldsymbol{\nabla}\cdot\boldsymbol{v} = 0, \tag{2.2}$$

$$\rho_\infty c_p(\boldsymbol{v}\cdot\boldsymbol{\nabla})T = \lambda\boldsymbol{\nabla}^2 T. \tag{2.3}$$

Here $\boldsymbol{e}_z = (0,0,1)$ is the unit vector in the z-direction and the velocity vector is given by $\boldsymbol{v} = (u,v,w)$. The deviation from a hydrostatic pressure field is denoted by p and T the temperature of the fluid. The material properties of the fluid $\rho_\infty, \mu, c_p, \lambda$ denote density, viscosity, specific heat and heat conductivity, which are all taken to be constant. The buoyant term features a linear dependence on temperature T around the reference density ρ_∞ (at T_∞). Volume expansion α and gravitational acceleration g are likewise constant.

The above conservation equations for momentum, mass and energy in the two-dimensional problem are subject to the boundary conditions

$$x, z \to \pm\infty : u \to 0, w \to w_\infty, T \to T_\infty, \tag{2.4p}$$

$$x = 0, |z| > \frac{d}{2} : u = 0, \frac{\partial w}{\partial x} = 0, \frac{\partial T}{\partial x} = 0, \tag{2.5p}$$

$$x \to \pm\infty, z : \frac{\partial u}{\partial x} \to 0, w \to w_\infty, T \to T_\infty, \tag{2.6p}$$

$$\sqrt{x^2 + z^2} = \frac{d}{2} : u = 0, w = 0, T = T_b. \tag{2.7p}$$

$$r, z \to \pm\infty : u \to 0, w \to w_\infty, T \to T_\infty, \tag{2.4a}$$

$$r = 0, |z| > \frac{d}{2} : u = 0, \frac{\partial w}{\partial r} = 0, \frac{\partial T}{\partial r} = 0, \tag{2.5a}$$

$$r \to \infty, z : \frac{\partial u}{\partial r} \to 0, w \to w_\infty, T \to T_\infty, \tag{2.6a}$$

$$\sqrt{r^2 + z^2} = \frac{d}{2} : u = 0, w = 0, T = T_b. \tag{2.7a}$$

Thus, we assume an undisturbed parallel and isothermal flow both far upstream and far downstream of the body. Symmetry with respect to both velocity and temperature fields is assumed with respect to the z-axis. On the body contour (cylinder, sphere) the no-slip condition and a constant temperature is applied. Sufficiently far aside of the body the flow is undisturbed with respect to w_∞ and T_∞, allowing in general a non-zero u in that region.

It is convenient at this stage to scale the problem in order to infer both dimensionless equations and dimensionless groups. We use the scales

$$(X, Z) = \frac{(x, z)}{d}, \tag{2.8p}$$

$$(R, Z) = \frac{(r, z)}{d}, \tag{2.8a}$$

$$(U, W) = \frac{(u, w)}{w_\infty}, \tag{2.9}$$

$$P = \frac{p}{\rho_\infty w_\infty^2}, \tag{2.10}$$

$$\Theta = \frac{(T - T_\infty)}{(T_b - T_\infty)}, \tag{2.11}$$

and, therefrom, obtain the dimensionless set of conservation equations

$$(\boldsymbol{V} \cdot \boldsymbol{\nabla})\boldsymbol{V} = -\boldsymbol{\nabla} P + \frac{1}{Re}\boldsymbol{\nabla}^2 \boldsymbol{V} + \frac{Gr}{Re^2}\Theta\, \boldsymbol{e_Z}, \tag{2.12}$$

$$\boldsymbol{\nabla} \cdot \boldsymbol{V} = 0, \tag{2.13}$$

$$(\boldsymbol{V} \cdot \boldsymbol{\nabla})\Theta = \frac{1}{PrRe}\boldsymbol{\nabla}^2 \Theta, \tag{2.14}$$

and boundary conditions

$$X, Z \to \pm\infty : U \to 0, W \to 1, \Theta \to 0, \tag{2.15p}$$

$$X = 0, |Z| > \frac{1}{2} : U = 0, \frac{\partial W}{\partial X} = 0, \frac{\partial \Theta}{\partial X} = 0, \tag{2.16p}$$

$$X \to \pm\infty, Z : \frac{\partial U}{\partial X} \to 0, W \to 1, \Theta \to 0, \tag{2.17p}$$

$$\sqrt{X^2 + Z^2} = \frac{1}{2} : U = 0, W = 0, \Theta = 1. \tag{2.18p}$$

$$R, Z \to \pm\infty : U \to 0, W \to 1, \Theta \to 0, \tag{2.15a}$$

$$R = 0, |Z| > \frac{1}{2} : U = 0, \frac{\partial W}{\partial R} = 0, \frac{\partial \Theta}{\partial R} = 0, \tag{2.16a}$$

$$R \to \infty, Z : \frac{\partial U}{\partial R} \to 0, W \to 1, \Theta \to 0, \tag{2.17a}$$

$$\sqrt{R^2 + Z^2} = \frac{1}{2} : U = 0, W = 0, \Theta = 1. \tag{2.18a}$$

The above scaling assumes the forced flow around the body to be dominant and, thus, uses the diameter d of the body, the far field velocity w_∞ and the dynamic pressure $(\rho_\infty w_\infty^2)$ to normalize length, velocity and pressure. The temperature scale is built up using the applied temperature difference $(T_b - T_\infty)$ such that $0 \leq \Theta \leq 1$ holds. The dimensionless groups in the above conservation equations (2.12-2.14) are identified as Reynolds number, Grashof number and Prandtl number. The definitions are

$$Re = \frac{w_\infty d}{\nu}, \tag{2.19}$$

$$Gr = \frac{\alpha g (T_b - T_\infty) d^3}{\nu^2}, \tag{2.20}$$

$$Pr = \frac{\nu}{\kappa} \tag{2.21}$$

The Reynolds number represents the ratio of inertia forces and viscous forces due to the forced flow. It, therefore, characterizes the strength of the forced flow in the problem. The Grashof number represents the ratio of the product of buoyancy forces and inertia forces and the square of viscous forces. It, thus, is a relative measure of the strength of the buoyant effects in the problem. Finally, the Prandtl number is the ratio of the transport coefficients of momentum and heat. The Prandtl number, therefore, is a fluid property, characterizing the fluid with respect to the molecular diffusion of momentum and heat.

The plane-flow behaviour, which we expect around a cylinder for pure forced-flow conditions is well known and has been discussed qualitatively in section 2.1. Using the Reynold number, we are now able to define the different regimes quantitatively. According to e.g. Žukauskas & Žiugžda (1985) we find in the range $Re < 1$ a steady flow around the cylinder without separation. In the range $3 < Re < 5$ the separation immediately behind the cylinder in conjunction with two symmetric vortices develops. Up to $Re < 40$ the flow remains steady and the size of the separation zone downstream increases. For $Re > 40$ the flow develops time-dependency in form of the so-called von-Kármán vortex street. This type of flow is characterized by periodic vortex detachment. The character of the near flow field around the cylinder to a first approximation is responsable for the type of flow in the wake. We can, therefore, conclude that under pure forced flow conditions we shall observe a steady plane wake behind the cylinder in the range $Re < 40$. That is precisely the range, which we shall restrict to in this article.

The axisymmetric flow behind a sphere behaves similarly. Following e.g. Lugt (1979) the flow remains attached in the range $Re < 20$. In the range $20 < Re < 400$ a torus shaped steady recirculating vortex behind the sphere is present and increases in size with increasing Re. For values $Re > 400$ unsteady behaviour develops. Thus, for the example of the sphere we can expect a steady flow in the near field for Reynolds numbers

$Re < 400$. If we, therefore, restrict the analysis to the range $Re < 400$ we shall observe a steady axisymmetric wake behind the sphere. In general bodies of more streamlined shape exhibit a wider range of Reynolds numbers, in which a steady wake, plane or axisymmetric, is observed. This is worth to notice, as the asymptotic model applies in the far wake for bodies of arbitrary shape. Thus, the range of validity for such bodies is fairly wide.

In principle, there are two possible reasons for a time-dependent wake. The first reason, of course, is the above described flow in the near field around the body. If that flow remains steady, there will be no excitation of the wake flow and from that source no time-dependency shall arrise. The second reason for a time-dependent wake might be an instability of the velocity profile in the wake further downstream. Following Betchov & Criminale (1967) inflection-type velocity profiles, as present in the wake, tend to go unstable for values $Re_{ip} > 200$. The Reynolds number Re_{ip} is defined based on the shear layer thickness $(\delta/2)$ and the velocity difference $[w_\infty - w(0,z)]$ in the wake. Thus, the definition is

$$Re_{ip} = \frac{[w_\infty - w(0,z)]\,\delta}{2\nu}. \tag{2.22}$$

As we shall restrict to steady wakes within this article, we have always to ensure that both conditions promise both a steady near field flow around the body and a stable (and thus steady) velocity profile in the wake further downstream. Given that, we can expect to a first approximation that the complete problem is steady. It remains at this stage, however, uncertain to which extend the buoyant acceleration of the fluid effects the stability of the velocity profiles in the wake. In general it is possible, that buoyant effects will shift the stability limit of the wake velocity profiles significantly. Similar effects of the buoyant forces onto the flow in the near field of the heated body may influence the steady/time-dependent transition. As we shall restrict to weakly-heated bodies throughout most of this article, we consider these effects to be of minor importance and judge the behaviour in time purely based on the forced flow stability limits.

2.3. *FEM simulation of the plane flow*

In order to obtain a full solution to the plane problem, we solve the above dimensionless equations (2.12-2.14) numerically, using the standard FEM code FIDAP 7.6. Although the boundary conditions (2.15-2.18) are mathematically formulated partly at infinite distances from the cylinder, we have to restrict the computational domain to a reasonable degree, while the appropriate boundary conditions now have to be formulated on the boundaries of the computational domain. Numerous tests have led us to chose the range of spatial coordinates for the numerical simulation as

$$0 \leq X \leq 30, \tag{2.23p}$$

$$-50 \leq Z \leq 60. \tag{2.24p}$$

Thus, for reason of symmetry, we discretize one half of the flow field and grid that region using nine-node quadrilateral elements, which employ biquadratic interpolation functions to approximate the velocity and temperature degrees of freedom within each element. The standard mesh for the computations is shown in figure 2. From the details of the mesh around the cylinder, which is given enlarged in figure 2, it is obvious that we employ mostly rectangular elements and only depart from rectangles in the immediate vincinity of the cylinder. Here, a transition region is constructed to integrate the cylinder geometry into the rectangular computational domain. The aspect ratio of

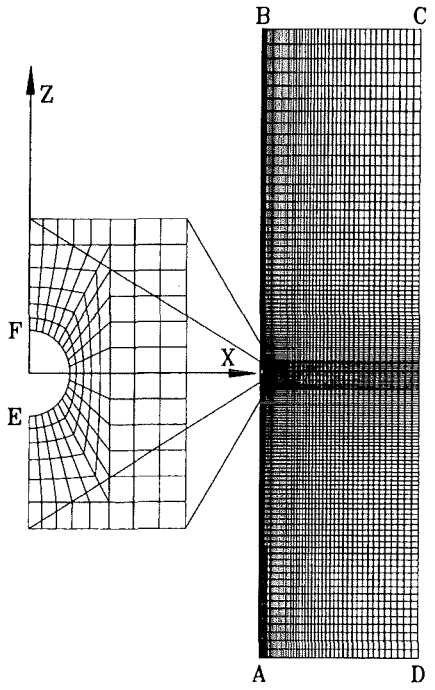

FIGURE 2. Employed FEM standard mesh

the elements has been kept close to one in all high gradient regions. Very few elements, in particular in the outlet plane $\overline{CB}$, have aspect ratios which depart from one and ratio at most 1:12. For standard computations we use about 6000 elements, corresponding to about 25,000 nodes, whereas numerous tests with strongly refined meshes and strongly increased computational domain have proven that all velocity and temperature profiles in the wake ($5 \leq Z \leq 50$) experience very little relative changes. Thus, we are confident that our standard mesh in extend and refinement guarantees a solution which is accurate to $\pm 0.2\%$. Typical computational efforts on an IBM RS/6000-580 workstation with 256 MB RAM range around 2000 CPU seconds.

We have in addition installed a procedure, which allows for an integration of all variables of the solution (and functions therefrom) along the 'open' boundaries of the computational domain, namely along $\overline{DC}$, $\overline{CB}$. This integration is based on the trapezoidal scheme and allows us e.g. to check quantitatively the integral mass balance, which always remains accurate to $\pm 0.1\%$. Moreover, this procedure allows us to infer, from the velocity and temperature on those boundaries, the integral amount of heat $\dot{q}$ (per unit length), which has actually been added to the flow. In similar fashion the integral balance with respect to the momentum flux is computed, which leads to a determination of the force (per unit length) f_z acting at the cylinder for the case of pure forced flow. The determination of $\dot{q}$ and f_z is essential as input for the asymptotic model, which will be described in the section below.

The boundary conditions which we apply to the computational domain, have for several reasons to depart from the ideal ones, formulated in equations (2.15-2.18). We use

$$0 \leq X \leq 30, Z = -50, (\overline{AD}) : U = 0, W = 1, \Theta = 0, \qquad (2.25p)$$

$$0 \leq X \leq 30, Z = 60, (\overline{BC}) : \frac{\partial U}{\partial Z} = 0, \frac{\partial W}{\partial Z} - \frac{Re}{2} P = 0, \frac{\partial \Theta}{\partial Z} = 0, \quad (2.26p)$$

$$X = 0, -50 \leq Z \leq -\frac{1}{2}, (\overline{AE}) : U = 0, \frac{\partial W}{\partial X} = 0, \frac{\partial \Theta}{\partial X} = 0, \quad (2.27p)$$

$$X = 0, \frac{1}{2} \leq Z \leq 60, (\overline{FB}) : U = 0, \frac{\partial W}{\partial X} = 0, \frac{\partial \Theta}{\partial X} = 0, \quad (2.28p)$$

$$X = 30, -50 \leq Z \leq 60, (\overline{CD}) : \frac{\partial U}{\partial X} = 0, \frac{\partial W}{\partial X} = 0, \Theta = 0, \quad (2.29p)$$

$$\sqrt{X^2 + Z^2} = \frac{1}{2}, (\overline{EF}) : U = 0, W = 0, \Theta = 1. \quad (2.30p)$$

Thus, mainly on the outflow boundary $\overline{BC}$ and the side boundary $\overline{CD}$ the conditions are modified, such that those boundary conditions do as little as possible influence the decaying profiles of velocities and temperature. The given set proves to behave in that manner.

2.4. *Asymptotic model for the far wake of weakly-heated bodies*

It is well known in literature (cf. Schlichting (1982)) that far laminar (and even turbulent) wakes behind bodies, both plane and axisymmetric, are well described using the boundary layer approximation. Similarly, buoyant plumes, in a sufficiently large distance above both line and point heat sources, allow for a theoretical modelling based on boundary layer theory. As both single effects in the problem develop a boundary layer type of flow sufficiently far downstream, it seems reasonable to expect that the combined and aligned occurance in a buoyant wake above a heated body likewise results in a flow field which has boundary-layer character.

A further idea on which this model is based is to assume that we have dominantly a forced flow, which develops a corresponding wake. As a disturbance to that flow we shall add weak heating, such that the contribution of the buoyant forces to the flow field remains small. This method allows to express the flow and temperature fields in a much simpler fashion if compared to the full problem, given in equations (2.12-2.18). It should be pointed out that the following asymptotic model holds for bodies of arbitrary shape of plane or axisymmetric geometry. This is a consequence of the far wake expansion, where the near field around the body is not resolved.

It occurs that both the far wake and the buoyant plume, whether plane or axisymmetric, within a boundary layer approximation will lead to a power-law dependency on the steamwise coordinate Z. As discussed e.g. by Berger (1971) for the far wake, the (singular) origin $Z = 0$ of this power law in general is not identical with the centre of the body, nor with the trailing edge. A similar statement should hold for the buoyant plume with respect to the (singular) heat source, particularly if the body has a finite extent. Taking the origin $Z = 0$ in the centre of the heated body, thus, in several respects is an approximation, while the error due to this approximation decays rapidly with increasing distance Z.

2.4.1. *Rescaling and boundary layer approximation*

If we focus on the boundary layer type of flow sufficiently far downstream above the body, it occurs reasonable to rescale the spatial coordinates such that the separate scales within the boundary layer are reflected. On one hand, within the far wake the diameter of the body d will not play an important role as a length scale, since the size and geometry of the body will only enter via an integral loss of momentum. On the other hand, the body diameter d is the only defined length and w_∞ the only defined velocity. Thus, we

maintain to some degree the scales given in equations (2.8-2.11), but rescale one of the spatial coordinates, by using the modified scales

$$\tilde{X} = \frac{x}{(d/\sqrt{Re})} = \sqrt{Re}\, X, \tag{2.31p}$$

$$\tilde{R} = \frac{r}{(d/\sqrt{Re})} = \sqrt{Re}\, R, \tag{2.31a}$$

$$\tilde{U} = \frac{u}{(w_\infty/\sqrt{Re})} = \sqrt{Re}\, U. \tag{2.32}$$

This separates the spatial scales by introducing the small parameter $\epsilon_1 = (1/\sqrt{Re})$. We furtheron take advantage of the smallness of ϵ_1, i.e. we restrict to the case

$$\sqrt{Re} \gg 1, \tag{2.33}$$

and readily infer the leading order of an asymptotic expansion of the conservation equations (2.12-2.14). Thus, we obtain the boundary layer equations for the problem, namely

$$\tilde{U}\frac{\partial W}{\partial \tilde{X}} + W\frac{\partial W}{\partial Z} = \frac{\partial^2 W}{\partial \tilde{X}^2} + \frac{Gr}{Re^2}\Theta + \mathcal{O}(\frac{1}{Re}), \tag{2.34p}$$

$$\frac{\partial \tilde{U}}{\partial \tilde{X}} + \frac{\partial W}{\partial Z} = 0, \tag{2.35p}$$

$$\tilde{U}\frac{\partial \Theta}{\partial \tilde{X}} + W\frac{\partial \Theta}{\partial Z} = \frac{1}{Pr}\frac{\partial^2 \Theta}{\partial \tilde{X}^2} + \mathcal{O}(\frac{1}{PrRe}); \tag{2.36p}$$

$$\tilde{U}\frac{\partial W}{\partial \tilde{R}} + W\frac{\partial W}{\partial Z} = \frac{\partial^2 W}{\partial \tilde{R}^2} + \frac{1}{\tilde{R}}\frac{\partial W}{\partial \tilde{R}} + \frac{Gr}{Re^2}\Theta + \mathcal{O}(\frac{1}{Re}), \tag{2.34a}$$

$$\frac{\partial(\tilde{R}\tilde{U})}{\partial \tilde{R}} + \frac{\partial(\tilde{R}W)}{\partial Z} = 0, \tag{2.35a}$$

$$\tilde{U}\frac{\partial \Theta}{\partial \tilde{R}} + W\frac{\partial \Theta}{\partial Z} = \frac{1}{Pr}\left(\frac{\partial^2 \Theta}{\partial \tilde{R}^2} + \frac{1}{\tilde{R}}\frac{\partial \Theta}{\partial \tilde{R}}\right) + \mathcal{O}(\frac{1}{PrRe}). \tag{2.36a}$$

As obvious from the above given accuracy of approximation within the heat transport equation (2.36), we restrict additionally to fluids with Prandtl numbers not too small, i.e. we assume

$$\sqrt{PrRe} \gg 1. \tag{2.37}$$

The boundary conditions within this approximation reduce to

$$\tilde{X} = 0, Z > 0 : U = 0, \frac{\partial W}{\partial \tilde{X}} = 0, \frac{\partial \Theta}{\partial \tilde{X}} = 0, \tag{2.38p}$$

$$\tilde{X} \to \pm\infty, Z > 0 : W \to 1, \Theta \to 0; \tag{2.39p}$$

$$\tilde{R} = 0, Z > 0 : U = 0, \frac{\partial W}{\partial \tilde{R}} = 0, \frac{\partial \Theta}{\partial \tilde{R}} = 0, \tag{2.38a}$$

$$\tilde{R} \to \infty, Z > 0 : W \to 1, \Theta \to 0. \tag{2.39a}$$

Since the asymptotic model is valid only far downstream of the body, the no-slip condition and the isothermal condition on the body contour cannot be enforced. Instead, we have to specify integral conditions for both the flux of momentum and the flux of heat. We pick a sufficiently large control volume around the body and balance mass, momentum and heat across the boundaries of the control volume. The drag force (respectively the drag force per unit length in the plane problem) is linked via

$$f_z = c_w \frac{\rho_\infty w_\infty^2}{2} d, \tag{2.40p}$$

$$F_z = c_w \frac{\rho_\infty w_\infty^2}{2} \frac{\pi d^2}{4}, \tag{2.40a}$$

to the dimensionless drag coefficient c_w, the dynamic pressure and the cross sectional area (respectively cross sectional area per unit length for the plane problem) of the body. At the centre of the body we allow additionally for the input of an integral heat flux $\dot{Q}$ (respectively an integral heat flux per unit length $\dot{q}$ for the plane problem) into the flow. Within the framework of boundary layer approximation the integral conditions for the flux of momentum and the flux of heat turn out to be

$$\frac{1}{2} c_w = \frac{f_z}{\rho_\infty w_\infty^2 d} = \frac{1}{\sqrt{Re}} \left[\int_{-\infty}^{\infty} W(1-W) d\tilde{X} + \frac{Gr}{Re^2} \int_{-\infty}^{Z} \int_{-\infty}^{\infty} \Theta d\tilde{X} dZ + \mathcal{O}(\frac{1}{Re}) \right], \tag{2.41p}$$

$$\Omega = \frac{\dot{q}}{\rho_\infty c_p (T_b - T_\infty)\nu} = \sqrt{Re} \left[\int_{-\infty}^{\infty} W \Theta d\tilde{X} + \mathcal{O}(\frac{1}{PrRe}) \right]; \tag{2.42p}$$

$$\frac{1}{16} c_w = \frac{F_z}{\rho_\infty w_\infty^2 2\pi d^2} = \frac{1}{Re} \left[\int_0^{\infty} \tilde{R} W(1-W) d\tilde{R} + \frac{Gr}{Re^2} \int_{-\infty}^{Z} \int_0^{\infty} \tilde{R} \Theta d\tilde{R} dZ + \mathcal{O}(\frac{1}{Re}) \right], \tag{2.41a}$$

$$\Omega = \frac{\dot{Q}}{\rho_\infty c_p d (T_b - T_\infty)\nu} = 2\pi \int_0^{\infty} \tilde{R} W \Theta d\tilde{R} + \mathcal{O}(\frac{1}{PrRe}). \tag{2.42a}$$

The dimensionless group Ω quantifies the integral amount of heat, transfered to the body. It is linked to the a Nusselt number, as shown in section 3.2.

2.4.2. *Asymptotic expansion for the far wake*

As we consider the development of the wake as the dominant physics in the problem, it is appropriate to invoke the approximations for the description of far wakes, as e.g. given by Schlichting (1982). This is, as we shall see, another asymptotic expansion in terms of the small parameter

$$\epsilon_2 = 1/\sqrt{Z}, \tag{2.43p}$$

$$\epsilon_2 = 1/Z. \tag{2.43a}$$

Formally, we apply the expansions

$$\tilde{U} = \epsilon_2 U_1 + \epsilon_2^2 U_2 + \ldots, \tag{2.44}$$

$$W = 1 - \epsilon_2 W_1 - \epsilon_2^2 W_2 + \ldots, \tag{2.45}$$

$$\Theta = \epsilon_2 \Theta_1 + \epsilon_2^2 \Theta_2 + \ldots, \tag{2.46}$$

which are strictly valid in the limit $\epsilon_2 \to 0$. At this stage we have to decide on the magnitude of the buoyant term in the momentum equations (2.34). As mentioned above, we shall consider only weak buoyant effects. Thus, we pick the Grashof number such that

$$\frac{Gr}{Re^2} = \mathcal{O}(\epsilon_2) \tag{2.47}$$

holds. This restricts the validity of the model with respect to large Gr. On the other hand it allows to shift the buoyant term into the second order of the expansion and, thus, provides a means of developing a solution. We shall discuss the range of validity of the model below in full detail. Using the expansions (2.44-2.46) and the above magnitude of Gr (cf. 2.47), we are able to break up the problem into a infinite number of simpler problems, whereas the two leading orders will be solved subsequently. The equations to first order are homogeneous and come to be

$$\frac{1}{\epsilon_2}\frac{\partial(\epsilon_2 W_1)}{\partial Z} - \frac{\partial^2 W_1}{\partial \tilde{X}^2} = 0, \tag{2.48p}$$

$$\frac{\partial U_1}{\partial \tilde{X}} - \frac{1}{\epsilon_2}\frac{\partial(\epsilon_2 W_1)}{\partial Z} = 0, \tag{2.49p}$$

$$\frac{1}{\epsilon_2}\frac{\partial(\epsilon_2 \Theta_1)}{\partial Z} - \frac{1}{Pr}\frac{\partial^2 \Theta_1}{\partial \tilde{X}^2} = 0; \tag{2.50p}$$

$$\frac{1}{\epsilon_2}\frac{\partial(\epsilon_2 W_1)}{\partial Z} - \left(\frac{\partial^2 W_1}{\partial \tilde{R}^2} + \frac{1}{\tilde{R}}\frac{\partial W_1}{\partial \tilde{R}}\right) = 0, \tag{2.48a}$$

$$\frac{\partial(\tilde{R} U_1)}{\partial \tilde{R}} - \frac{\tilde{R}}{\epsilon_2}\frac{\partial(\epsilon_2 W_1)}{\partial Z} = 0, \tag{2.49a}$$

$$\frac{1}{\epsilon_2}\frac{\partial(\epsilon_2 \Theta_1)}{\partial Z} - \frac{1}{Pr}\left(\frac{\partial^2 \Theta_1}{\partial \tilde{R}^2} + \frac{1}{\tilde{R}}\frac{\partial \Theta_1}{\partial \tilde{R}}\right) = 0, \tag{2.50a}$$

with the corresponding boundary and integral conditions

$$\tilde{X} = 0, Z > 0 : U_1 = 0, \frac{\partial W_1}{\partial \tilde{X}} = 0, \frac{\partial \Theta_1}{\partial \tilde{X}} = 0, \tag{2.51p}$$

$$\tilde{X} \to \pm\infty, Z > 0 : W_1 \to 0, \Theta_1 \to 0, \tag{2.52p}$$

$$\int_{-\infty}^{\infty} W_1 d\tilde{X} = \frac{c_w}{2}\sqrt{Re}\sqrt{Z}, \tag{2.53p}$$

$$\int_{-\infty}^{\infty} \Theta_1 d\tilde{X} = \frac{\Omega\sqrt{Z}}{\sqrt{Re}}; \tag{2.54p}$$

$$\tilde{R} = 0, Z > 0 : U_1 = 0, \frac{\partial W_1}{\partial \tilde{R}} = 0, \frac{\partial \Theta_1}{\partial \tilde{R}} = 0, \tag{2.51a}$$

$$\tilde{R} \to \infty, Z > 0 : W_1 \to 0, \Theta_1 \to 0, \tag{2.52a}$$

$$\int_{0}^{\infty} \tilde{R} W_1 d\tilde{R} = \frac{c_w}{16} Re\, Z, \tag{2.53a}$$

$$\int_{0}^{\infty} \tilde{R}\Theta_1 d\tilde{R} = \frac{\Omega}{2\pi} Z. \tag{2.54a}$$

This set of equations (2.48-2.54) can be solved analytically by introducing the similarity variable

$$\eta = \frac{\tilde{X}}{\sqrt{Z}}, \tag{2.55p}$$

$$\eta = \frac{\tilde{R}}{\sqrt{Z}}. \tag{2.55a}$$

Using η the solution is

$$U_1 = -\frac{c_w\sqrt{Re}}{8\sqrt{\pi}\sqrt{Z}}\,\eta\,\exp\left(-\frac{\eta^2}{4}\right), \tag{2.56p}$$

$$W_1 = \frac{c_w\sqrt{Re}}{4\sqrt{\pi}}\,\exp\left(-\frac{\eta^2}{4}\right), \tag{2.57p}$$

$$\Theta_1 = \frac{\Omega\sqrt{Pr}}{2\sqrt{\pi}\sqrt{Re}}\,\exp\left(-Pr\,\frac{\eta^2}{4}\right); \tag{2.58p}$$

$$U_1 = -\frac{c_w Re}{64\sqrt{Z}}\,\eta\,\exp\left(-\frac{\eta^2}{4}\right), \tag{2.56a}$$

$$W_1 = \frac{c_w Re}{32}\,\exp\left(-\frac{\eta^2}{4}\right), \tag{2.57a}$$

$$\Theta_1 = \frac{\Omega Pr}{4\pi}\,\exp\left(-Pr\,\frac{\eta^2}{4}\right). \tag{2.58a}$$

With respect to the flow field, this solution is equivalent to the results for the linearized

far wake, given in the literature (e.g. Schlichting (1982), Loitsianski (1967)). The temperature field within this approximation reflects the passive transport of the added heat due to diffusion and convection, based on the undisturbed, parallel flow. Of course, no coupling (via buoyancy forces) of the temperature field towards the flow field is present.

Within the second order the equations turn non-homogeneous, whereas the inhomogenity is governed by non-linearities and the buoyant term. The conservation equations, thus, read

$$\frac{1}{\epsilon_2^2}\frac{\partial(\epsilon_2^2 W_2)}{\partial Z} - \frac{\partial^2 W_2}{\partial \tilde{X}^2} = -\frac{c_w^2 Re}{32\pi Z}\exp\left(-\frac{\eta^2}{2}\right) - \frac{\Omega Gr\sqrt{Pr}\sqrt{Z}}{2\sqrt{\pi}Re^{5/2}}\exp\left(-Pr\frac{\eta^2}{4}\right), \quad (2.59p)$$

$$\frac{\partial U_2}{\partial \tilde{X}} - \frac{1}{\epsilon_2^2}\frac{\partial(\epsilon_2^2 W_2)}{\partial Z} = 0, \quad (2.60p)$$

$$\frac{1}{\epsilon_2^2}\frac{\partial(\epsilon_2^2 \Theta_2)}{\partial Z} - \frac{1}{Pr}\frac{\partial^2 \Theta_2}{\partial \tilde{X}^2} = -\frac{c_w \Omega\sqrt{Pr}}{16\pi Z}\exp\left(-(1+Pr)\frac{\eta^2}{4}\right); \quad (2.61p)$$

$$\frac{1}{\epsilon_2^2}\frac{\partial(\epsilon_2^2 W_2)}{\partial Z} - \left(\frac{\partial^2 W_2}{\partial \tilde{R}^2} + \frac{1}{\tilde{R}}\frac{\partial W_2}{\partial \tilde{R}}\right) = -\frac{c_w^2 Re^2}{1024 Z}\exp\left(-\frac{\eta^2}{2}\right) - \frac{\Omega GrPrZ}{4\pi Re^2}\exp\left(-Pr\frac{\eta^2}{4}\right), \quad (2.59a)$$

$$\frac{\partial(RU_2)}{\partial \tilde{R}} - \frac{\tilde{R}}{\epsilon_2^2}\frac{\partial(\epsilon_2^2 W_2)}{\partial Z} = 0, \quad (2.60a)$$

$$\frac{1}{\epsilon_2^2}\frac{\partial(\epsilon_2^2 \Theta_2)}{\partial Z} - \frac{1}{Pr}\left(\frac{\partial^2 \Theta_2}{\partial \tilde{R}^2} + \frac{1}{\tilde{R}}\frac{\partial \Theta_2}{\partial \tilde{R}}\right) = -\frac{c_w \Omega PrRe}{128\pi Z}\exp\left(-(1+Pr)\frac{\eta^2}{4}\right). \quad (2.61a)$$

The corresponding boundary and integral conditions are

$$\tilde{X} = 0, Z > 0 : U_2 = 0, \frac{\partial W_2}{\partial \tilde{X}} = 0, \frac{\partial \Theta_2}{\partial \tilde{X}} = 0, \quad (2.62p)$$

$$\tilde{X} \to \pm\infty, Z > 0 : W_2 \to 0, \Theta_2 \to 0, \quad (2.63p)$$

$$\int_{-\infty}^{\infty} W_2 d\tilde{X} = \frac{\sqrt{2}c_w^2 Re\sqrt{Z}}{16\sqrt{\pi}} - \frac{\Omega GrZ^2}{Re^{5/2}} - \frac{Gr\Delta mZ}{Re^2}, \quad (2.64p)$$

$$\int_{-\infty}^{\infty} \Theta_2 d\tilde{X} = \frac{c_w \Omega\sqrt{Z}}{4\sqrt{\pi}}\sqrt{\frac{Pr}{1+Pr}}; \quad (2.65p)$$

$$\tilde{R} = 0, Z > 0 : U_2 = 0, \frac{\partial W_2}{\partial \tilde{R}} = 0, \frac{\partial \Theta_2}{\partial \tilde{R}} = 0, \quad (2.62a)$$

$$\tilde{R} \to \infty, Z > 0 : W_2 \to 0, \Theta_2 \to 0, \quad (2.63a)$$

$$\int_0^\infty \tilde{R} W_2 d\tilde{R} = \frac{c_w^2 Re^2 Z}{1024} - \frac{\Omega Gr Z^3}{6\pi Re^2} - \frac{Gr\Delta m Z^2}{Re^2}, \tag{2.64a}$$

$$\int_0^\infty \tilde{R}\Theta_2 d\tilde{R} = \frac{c_w \Omega Re Z}{64\pi} \frac{Pr}{1+Pr}. \tag{2.65a}$$

Δm denotes the constant of integration, which occurs by integrating the temperature field in equation (2.41). Here the integral of the buoyant forces across the entire control volume is required. Since the true temperature $\Theta(\tilde{X}, Z)$ is not known in the near field, we replace the definite integral with respect to Z in equation (2.41) by an indefinite integral.

With respect to the flow field the set of equations (2.59-2.65) introduces nonlinearities of the convective terms and includes the weak buoyant forces, resulting from the first order temperature field. For the non-buoyant far wake flow, i.e. in the limit $Gr \to 0$, the above equations agree with the second order expansion of Goldstein (1933). The convective temperature transport within this approximation is based on the first order wake velocity profiles. It is, however, important to keep in mind that buoyant effects are still dependent on the first order temperature field, i.e. the wake flow field does not yet recouple via the buoyant forces.

We transform the set of equations (2.59-2.65) to a corresponding set of ordinary differential equations by means of the similarity transformation

$$U_2 = \frac{\sqrt{2} c_w^2 Re}{16\sqrt{\pi}\sqrt{Z}} G(\eta) + \frac{\Omega Gr Z}{Re^{5/2}} I(\eta) + \frac{Gr\Delta m}{4\sqrt{\pi} Re^2} \eta \exp\left(-\frac{\eta^2}{4}\right), \tag{2.66p}$$

$$W_2 = \frac{\sqrt{2} c_w^2 Re}{16\sqrt{\pi}} F(\eta) + \frac{\Omega Gr Z^{3/2}}{Re^{5/2}} K(\eta) - \frac{Gr\Delta m\sqrt{Z}}{2\sqrt{\pi} Re^2} \exp\left(-\frac{\eta^2}{4}\right), \tag{2.67p}$$

$$\Theta_2 = \frac{c_w \Omega}{4\sqrt{\pi}} \sqrt{\frac{Pr}{1+Pr}} H(\eta); \tag{2.68p}$$

$$U_2 = \frac{c_w^2 Re^2}{1024\sqrt{Z}} G(\eta) + \frac{\Omega Gr Z^{3/2}}{6\pi Re^2} I(\eta) + \frac{Gr\Delta m\sqrt{Z}}{4Re^2} \eta \exp\left(-\frac{\eta^2}{4}\right), \tag{2.66a}$$

$$W_2 = \frac{c_w^2 Re^2}{1024} F(\eta) + \frac{\Omega Gr Z^2}{6\pi Re^2} K(\eta) - \frac{Gr\Delta m Z}{2Re^2} \exp\left(-\frac{\eta^2}{4}\right), \tag{2.67a}$$

$$\Theta_2 = \frac{c_w \Omega Re}{64\pi} \frac{Pr}{1+Pr} H(\eta). \tag{2.68a}$$

This generalized transformation leads to a set ordinary differential equations for the shape functions $G(\eta), I(\eta), F(\eta), K(\eta), H(\eta)$, which is readily inferred to be

$$F'' + \frac{\eta}{2} F' + F = \frac{1}{\sqrt{8\pi}} \exp\left(-\frac{\eta^2}{2}\right), \tag{2.69p}$$

$$K'' + \frac{\eta}{2} K' - \frac{1}{2} K = \frac{\sqrt{Pr}}{2\sqrt{\pi}} \exp\left(-Pr\frac{\eta^2}{4}\right), \tag{2.70p}$$

$$G' + \frac{\eta}{2}F' + F = 0, \tag{2.71p}$$

$$I' + \frac{\eta}{2}K' - \frac{1}{2}K = 0, \tag{2.72p}$$

$$H'' + Pr\,\frac{\eta}{2}H' + PrH = \frac{Pr\sqrt{1+Pr}}{4\sqrt{\pi}}\,\exp\left(-(1+Pr)\frac{\eta^2}{4}\right); \tag{2.73p}$$

$$F'' + \left(\frac{\eta}{2} + \frac{1}{\eta}\right)F' + 2F = \exp\left(-\frac{\eta^2}{2}\right), \tag{2.69a}$$

$$K'' + \left(\frac{\eta}{2} + \frac{1}{\eta}\right)K' = \exp\left(-Pr\,\frac{\eta^2}{4}\right), \tag{2.70a}$$

$$G' + \frac{1}{\eta}G + \frac{\eta}{2}F' + 2F = 0, \tag{2.71a}$$

$$I' + \frac{1}{\eta}I + \frac{\eta}{2}K' = 0, \tag{2.72a}$$

$$H'' + \left(Pr\,\frac{\eta}{2} + \frac{1}{\eta}\right)H' + 2Pr\,H = \frac{Pr\,(1+Pr)}{2}\,\exp\left(-(1+Pr)\frac{\eta^2}{4}\right). \tag{2.73a}$$

The corresponding boundary and integral conditions are

$$\eta = 0 : I = 0, G = 0, F' = 0, K' = 0, H' = 0, \tag{2.74}$$

$$\eta \to \pm\infty : F \to 0, K \to 0, H \to 0, \tag{2.75}$$

$$\int_{-\infty}^{\infty} F d\eta = 1, \tag{2.76p}$$

$$\int_{-\infty}^{\infty} K d\eta = -1, \tag{2.77p}$$

$$\int_{-\infty}^{\infty} H d\eta = 1; \tag{2.78p}$$

$$\int_{0}^{\infty} \eta F d\eta = 1, \tag{2.76a}$$

$$\int_{0}^{\infty} \eta K d\eta = -1, \tag{2.77a}$$

$$\int_{0}^{\infty} \eta H d\eta = 1. \tag{2.78a}$$

We apply a multiple shooting method, based on a fourth order Runge-Kutta scheme for the integration of the associated initial value problem, to solve the above set of ordinary

differential equations, boundary and integral conditions (2.69-2.78). Given a solution to the shape functions, we can summarize the results for the flow and temperature fields as follows

$$\tilde{U} = -\frac{\bar{c}_w\sqrt{Re}}{8\sqrt{\pi}Z}\,\eta\,\exp\left(-\frac{\eta^2}{4}\right) + \frac{\sqrt{2}\bar{c}_w^2 Re}{16\sqrt{\pi}Z^{3/2}}G(\eta) + \frac{\Omega Gr}{Re^{5/2}}I(\eta) + \ldots, \tag{2.79p}$$

$$W = 1 - \frac{\bar{c}_w\sqrt{Re}}{4\sqrt{\pi}\sqrt{Z}}\,\exp\left(-\frac{\eta^2}{4}\right) - \frac{\sqrt{2}\bar{c}_w^2 Re}{16\sqrt{\pi}Z}F(\eta) - \frac{\Omega Gr\sqrt{Z}}{Re^{5/2}}K(\eta) + \ldots, \tag{2.80p}$$

$$\Theta = \frac{\Omega\sqrt{Pr}}{2\sqrt{\pi}\sqrt{Re}\sqrt{Z}}\,\exp\left(-Pr\,\frac{\eta^2}{4}\right) + \frac{\bar{c}_w\Omega}{4\sqrt{\pi}Z}\sqrt{\frac{Pr}{(1+Pr)}}\,H(\eta) + \ldots; \tag{2.81p}$$

$$\tilde{U} = -\frac{\bar{c}_w Re}{64Z^{3/2}}\,\eta\,\exp\left(-\frac{\eta^2}{4}\right) + \frac{\bar{c}_w^2 Re^2}{1024Z^{5/2}}G(\eta) + \frac{\Omega Gr}{6\pi Re^2\sqrt{Z}}I(\eta) + \ldots, \tag{2.79a}$$

$$W = 1 - \frac{\bar{c}_w Re}{32Z}\,\exp\left(-\frac{\eta^2}{4}\right) - \frac{\bar{c}_w^2 Re^2}{1024Z^2}F(\eta) - \frac{\Omega Gr}{6\pi Re^2}K(\eta) + \ldots, \tag{2.80a}$$

$$\Theta = \frac{\Omega Pr}{4\pi Z}\,\exp\left(-Pr\,\frac{\eta^2}{4}\right) + \frac{\bar{c}_w\Omega Re}{64\pi Z^2}\frac{Pr}{(1+Pr)}\,H(\eta) + \ldots\,. \tag{2.81a}$$

Within equations (2.80) we have introduced an effective drag coefficient $\bar{c}_w$, defined by

$$\bar{c}_w = c_w - \frac{2Gr\Delta m}{Re^{5/2}}, \tag{2.82p}$$

$$\bar{c}_w = c_w - \frac{16Gr\Delta m}{Re^3}. \tag{2.82a}$$

The effective drag coefficient $\bar{c}_w$ includes both the forced flow drag coefficient c_w of the body and the constant of integration Δm. For an isothermal flow $\bar{c}_w = c_w$ is obvious.

2.4.3. *Limitations of the model*

At this stage it seems reasonable to summarize the assumptions and limitations which restrict the range of validity of the above model. Firstly, applying the boundary layer approximation within both the transport equations of momentum and heat restricts us to the range of large Reynolds numbers and fluids featuring not too small Prandtl numbers. Thus we have to have

$$\sqrt{Re} \gg 1, \tag{2.83}$$

$$\sqrt{PrRe} \gg 1. \tag{2.84}$$

Secondly, the far wake approximation restricts to large Z. To be precise, given the actual Reynolds number, we infer from the approximative solution (2.80), that the expansion holds if

$$\sqrt{Z} \gg \frac{\bar{c}_w\sqrt{Re}}{4\sqrt{\pi}}, \tag{2.85p}$$

$$Z \gg \frac{\bar{c}_w Re}{32}, \tag{2.85a}$$

is fullfilled. Thirdly, we have a limitation from the assumption of a weakly-heated body. The buoyant contributions in (2.80) remain small if

$$\Omega Gr \ll \frac{Re^{5/2}}{\sqrt{Z}}, \tag{2.86p}$$

$$\Omega Gr \ll 6\pi Re^2, \tag{2.86a}$$

holds.

Conditions (2.83,2.84) are immediately transparent, in that a sufficiently large Reynolds number is required. Conditions (2.85,2.86) per se are likewise physically clear as weak buoyant effects are considered. However, the combined application of conditions (2.85p) and (2.86p) for the plane problem gives

$$\frac{\bar{c}_w \sqrt{Re}}{4\sqrt{\pi}} \ll \sqrt{Z} \ll \frac{Re^{5/2}}{\Omega Gr}. \tag{2.87p}$$

This is different for the axisymmetric problem, where Z is allowed in a range

$$\frac{\bar{c}_w Re}{32} \ll Z \ll \infty. \tag{2.87a}$$

Particularly condition (2.87p) is an unexpected result, which is caused by the growth of the buoyant term downstream for the plane case (cf. equation (2.80p)).

3. Experimental methods

We aim to assess experimental data for the laminar mixed convective flow in the wake of a heated body. We restrict our experiment to a plane situation in that we pick a heated cylinder and realize a plane flow and temperature field in the wake above this cylinder. We, therefore, have to establish a homogeneous laminar flow, rising in a vertical channel. This flow has to be controlled carefully with respect to flow rate and temperature. We have, finally, to control the temperature of the cylinder. The measuring technique has to monitor the flow and temperature fields in the wake above the cylinder to allow for a quantitative comparison of the experimental situation with the theoretical predictions. Based on the above ideas, we have designed the experimental channel, which is described in detail in the following chapter.

3.1. *Setup and measuring technique*

The actual test section is sketched in figure 3. Water enters the test channel at a well controlled temperature T_∞ from below via two horizontal pipes, which are perforated to allow for a horizontal outlet, homogeneously into the lowest chamber. Through a sequence of two honeycomb inserts (H_1, H_2) and two fine screens (S_1, S_2), in conjunction with the contraction (cf. figure 3), the flow is made parallel and homogeneous across most of the channels cross section. Leaving the most upper screen S_2, the flow passes the cylinder of diameter $d = 6\,mm$. The channel in that region has parallel walls and a square cross section of $30 \times 30\,cm$. The water leaves the channel after a length of about $50\,cm$ via a free interface outflow. A constant integral flow rate through the test channel and a constant entrance temperature of the water is achieved by a controlled pump, a

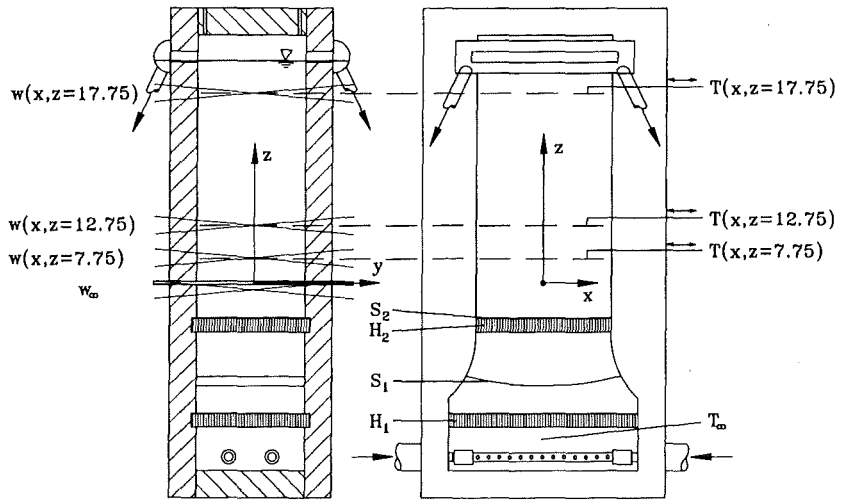

FIGURE 3. Sketch of the test section and measuring technique

complete insulation of the test channel and all elements of the water circuit and two heat exchangers, which see an extremely carefully controlled temperature at their secondary side. These measures allow to keep the velocity w_∞ in the cylinder plane constant to $\pm 1\%$ and the inlet temperature T_∞ constant to $\pm 0.05\ degC$. The cylinder is likewise kept at constant temperature T_b. This is achieved by circulating water of constant temperature through a pipe of $6\ mm$ outer diameter, which gives a temperature constance of about $\pm 0.02\ degC$.

The measuring technique consists of a number of thermocouples mounted on traversing drives, which allow for the measurement of temperature profiles $T_i(x)$ at three distances z_1, z_2, z_3 above the cylinder. In dimensionless scale, those planes are located at $Z_1 = 7.75, Z_2 = 12.75, Z_3 = 17.75$. The temperature profiles $T_i(x)$ are taken in the middle of the channel, where an almost undisturbed plane situation is present. Moreover, the homogenity of temperature T_∞ in the plane of the most upper screen S_2 is monitored by another three thermocouples at different positions. All temperature measurements are taken in difference to the inlet temperature T_∞, which is picked within a copper cube of $3cm$ side length positioned within the lowest chamber. Additionally three PT100 resistant thermometers monitor at higher accuracy the cylinder temperature at two positions and once more the inlet temperature T_∞. Accuracy of the thermocouple difference measurements is $\pm 0.05\ degC$, while the PT100 probes are typically accurate to $\pm 0.01\ degC$.

The flow field is registered using two one-component Laser Doppler Anemometers. The first LDA maesuring volume is at a fixed point between the cylinder axis and the channel wall. The orientation is such that the undisturbed velocity w_∞ is measured using the forward scattered light. The second LDA features a relatively small optical head connected via fiber optics to a stationary unit with Laser, Bragg cell, photomultipliers, etc. . Its maesuring volume is traversed along identical lines as described for the thermocouples by means of another stepping motor drive. The orientation is such that profiles $w_i(x)$ are measured at three distances z_1, z_2, z_3 above the cylinder, while in this case the backscattered light is picked up by the optical head. Likewise these velocity profiles are taken in the middle of the channel to focus mainly on plane effects. Precision of both LDA measuring systems, due to a sophisticated transient recorder based evaluation of the signals should range around $\pm 0.2 mm/s$, positioning of traversing drives (velocity and

property	symbol	value	units
density	ρ_∞	$9.9705 \cdot 10^2$	$kg\, m^{-3}$
specific heat	c_p	$4.1790 \cdot 10^3$	$Ws\, kg^{-1}K^{-1}$
thermal expansion	α	$2.5720 \cdot 10^{-4}$	K^{-1}
heat conductivity	λ	$6.0720 \cdot 10^{-5}$	$W\, m^{-1}K^{-1}$
viscosity	ν	$8.9300 \cdot 10^{-7}$	$m^2 s^{-1}$

TABLE 1. Properties of the test liquid (water) for $T_0 = 25degC, p_0 = 1bar$

temperature probes) is highly accurate to $\pm 0.01\, mm$. Typically, profiles of temperature and velocity are taken in steps down to $\Delta x = 1\, mm$.

3.2. *Scaling and preliminary measurements*

In order to apply the asymptotic model to the experimental conditions we need to determine several (integral) parameters, namely the dimensionless groups $Re, c_w, \bar{c}_w, Gr, \Omega, Pr$. Moreover, the quantities in the scaling relations (2.8-2.11) w_∞, T_b, T_∞ need to be determined. The temperatures T_b and T_∞ of the cylinder and of the fluid upstream are directly available from measurements. Thus, as T_∞ is kept constant at $T_\infty = 25degC$ all liquid properties $\rho_\infty, c_p, \alpha, \lambda, \nu$ are known. These properties are summarized in table 1. The velocity w_∞ is directly measured by the stationary LDA system in height of the cylinder ($Z = 0$). As we have a finite cross section of the channel, the no-slip condition leads to the development of kinematic boundary layers at all four vertical walls downstream of the last screen insert S_2. For reasons of continuity, the presence of low velocity regions at the walls causes inreased velocity amplitudes in the intermediate region between the wake and the wall boundary layers. As the wall boundary layers increase in thickness downstream, an acceleration of the flow in the intermediate region is the consequence. Thus, in the measuring planes $Z_i = 7.75, 12.75, 17.75$ we expect values $w_{\infty,i} > w_\infty$ in the outer region. In fact, we find due to these imperfections an increase of w_∞ by about 18% along the channel. For scaling of the velocity profiles we therefore use the spatially averaged plateau value $w_{\infty,i}$ in the outer region of the respective plane Z_i, which typically occurs in a region $|X| > 4$. For the determination of the Reynolds number Re (cf. eq. (2.19)), in contrast, we use an averaged value from the two planes $Z = 0$ and $Z = 17.75$.

The drag coefficient c_w of the cylinder for forced flow conditions depends purely on the Reynolds number Re. Schlichting (1982) gives for our experimental Reynolds number $Re = 39.4$ a value of $c_w = 1.8$. It is alternatively possible to use our numerical (FEM) results for the determination of c_w. This can be achieved by two methods, namely by an integration of the stress field around the cylinder contour, which provides both components of the acting force $\boldsymbol{f}$ per unit length. From the vertical component f_z the drag coefficient c_w can be computed by means of equation (2.40p). The second method engages in an integral momentum balance of the entire computational domain. This method is outlined in section 2.3 and provides likewise a value for c_w. The values obtained from these two methods for forced-flow conditions are $c_w = 1.475, 1.499$. All values are given in figure 4a for $Gr = 0$.

For mixed-convection conditions we may still use an integration of the stress field around the cylinder contour to determine the force, and thus c_w, acting at the heated cylinder ($Gr > 0$). Using this method we find increasing values of c_w for increasing Grashof numbers Gr (cf. circles in figure 4a). An inspection of the flow field reveals that this increase of drag is due to the disappearance of the recirculation zone behind the cylinder. Thus, for large Grashof numbers the flow is attached to the complete cylinder

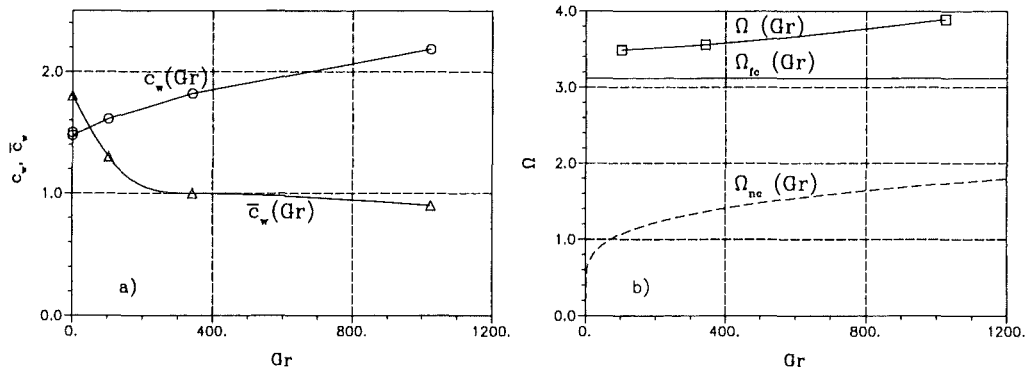

FIGURE 4. Drag coefficient c_w, effective drag coefficient $\bar{c}_w$ and heat transfer coefficient Ω as function of Gr

contour and a stronger interaction occurs. The integral momentum balance around the computational domain, of course, is not suitable to determine c_w in a non-isothermal situation. Here only the sum of all acting forces (including buoyant forces) is obtained.

As inferred in section 2.4.2, the asymptotic model is based on an effective drag coefficient $\bar{c}_w$, defined by equation (2.82p). The constant of integration Δm in equation (2.82p) is strictly constant with respect to the spatial coordinates $\tilde{X}, Z, \eta$. The values $\bar{c}_w$ employed within the asymptotic model for different Grashof numbers are given in figure 4a as triangles. These values are inferred from the corresponding FEM simulations. For small Grashof numbers a linear decrease of $\bar{c}_w$ with increasing Gr is obvious, precisely as predicted by equation (2.82p). The departure from the linear behaviour for large Gr is not surprising, as Δm develops a dependency on Gr. In this range of large Grashof numbers the asymptotic model is no longer valid.

The Prandtl number Pr is available from the fluid properties given in table 1. At a reference temperature of $T_\infty = 25 degC$ we find $Pr = 6.128$. Within the asymptotic model the heat input is encoded in the parameters Gr and Ω. The Grashof number is readily computed from the fluid properties and the measured temperatures T_b, T_∞. The dimensionless heat transfer coefficient Ω is linked to the Nusselt number Nu and quantifies the integral heat transfer. In fact, we have used our numerical (FEM) results to determine the transferred heat $\dot{q}$. The method is outlined in section 2.3. Based on $\dot{q}$ we determine Ω via equation (2.42p). The obtained values Ω for various Grashof numbers are plotted in figure 4b as squares. An increase of Ω with increasing Gr is obvious. We check these heat transfer data by using literature correlations for the forced flow and natural convective flow heat transfer from a cylinder. Following Gnielinski (1975) and Churchill & Chu (1975) for laminar flow the empirical correlations

$$\Omega_{fc} = 2Nu\ Pr^{-1} = 1.6644\ Re^{1/2} Pr^{-2/3}, \tag{3.1}$$

$$\Omega_{nc} = 2Nu\ Pr^{-1} = 2Pr \left[0.6 + \frac{0.387(PrGr)^{1/6}}{\left(1 + \left(\frac{0.559}{Pr}\right)^{9/16}\right)^{8/27}} \right]^2, \tag{3.2}$$

hold. For the specific Reynolds and Prandtl numbers in the experiment $Re = 39.4$, $Pr = 6.128$ the correlations yield

$$\Omega_{fc} = 3.12, \tag{3.3}$$

$$\Omega_{nc} = \left(0.43 + 0.279 Gr^{1/6}\right)^2. \tag{3.4}$$

The Nusselt number is defined by

$$Nu = \frac{\pi}{2}\frac{h\,d}{\lambda}, \tag{3.5}$$

where h is the heat transfer coefficient. Both Ω_{fc} and Ω_{nc} are given in figure 4b by solid and dashed lines. Our results from the FEM simulations for Ω (cf. squares in figure 4b) compare reasonably well with the correlations (3.3,3.4). Firstly, the value Ω_{fc} is about 10% lower than the extrapolated value for $Gr \to 0$ from our data. Secondly, the increase of Ω with increasing Gr occurs perfectly parallel to the increase of Ω_{nc} in correlation (3.4). The curve $\Omega_{nc}(Gr)$ is shifted to lower values, though. This is due to the presence of the forced flow within the present heat transfer data in figure 4b (symbols □).

4. Results

In the following sections we shall give results obtained for the flow field in various parameter regimes. As we intend to compare with plane experiments, we restrict ourselves to the plane problem below. We shall mainly focus on the dimensionless vertical velocity profiles $W(X, Z_i)$ in three different planes downstream, above the cylinder. In fact, temperature profiles $\Theta(X, Z_i)$ of reasonable quality have only be obtained for the case of a strongly-heated cylinder. Thus, the discussion of the temperature field remains restricted to this case.

The isothermal problem is discussed to check the various results from the experiments, the asymptotic model and the numerical (FEM) simulations for consistency. Here, the particular aspects of the forced flow can be verified, such as the development of the far (and near) wake. This part does not contain new results, as all features of far wakes presented here are well known in literature (e.g. Berger (1971)). The part related to the weakly-heated cylinder is devoted to verify the particular aspects of weak buoyant forces within the asymptotic model. Thus, the parameters are chosen such, that the asymptotic model applies. Finally, the part related to the stongly-heated cylinder gives results for parameter regimes outside the validity range of the asymptotic model. Here mixed convection with strong buoyant forces is present and only a comparison of experimental findings and numerical (FEM) simulations occurs reasonable.

4.1. *Isothermal wake*

In figure 5 our results for the flow field are collated for an isothermal situation. We recognize in figure 5a measured vertical velocity profiles $W(X, Z_i)$ in three planes Z_i above the cylinder. The data points are given on both sides of the symmetry line $X = 0$ in addition to least-square fits of the symmetric form

$$W = 1 - C_1 \exp\left(C_2 X^2\right). \tag{4.1}$$

We recognize in the plane $Z = 7.75$ (symbols ▽) a pronounced wake profile with a substantial velocity deficit on the centre line $X = 0$. As we move downstream to $Z = 12.75, 17.75$ (symbols □, ○) the velocity deficit decreases. Moreover, the width of

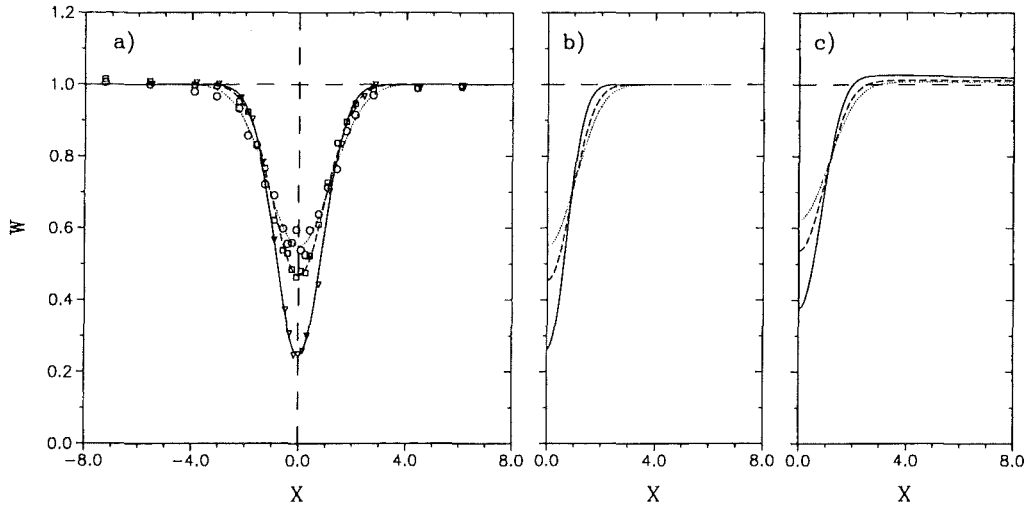

FIGURE 5. Profiles of the dimensionless vertical velocity $W(X, Z_i)$ downstream of an isothermalal cylinder. a) gives the experimental data and corresponding least-square fits, b) gives results from the asymptotic theory and c) gives results from the numerical simulations. The distances above the cylinder are $Z_i = 7.75, 12.75, 17.75$, the parameters are $Re = 39.4, c_w = \bar{c}_w = 1.8$.

the wake (in X) increases downstream. Employing equation (2.85p) we can estimate the small parameter in the asymptotic representation to be

$$\frac{\bar{c}_w\sqrt{Re}}{4\sqrt{\pi}\sqrt{Z_i}} = 0.57, 0.45, 0.38, \tag{4.2}$$

for the planes $Z_i = 7.75, 12.75, 17.75$. Thus, particularly for Z_1 the asymptotic representation may be critical.

Figure 5c shows the corresponding profiles obtained by means of the numerical (FEM) simulations. Here the identical features of the wake are observed, namely a widening and a fill-up of the wake profile with increasing Z. Quantitatively, two characteristic differences arise in comparison with the experimental profiles in figure 5a. Firstly, the numerical simulations give velocities $W > 1$ ouside the wake. In contrast, the experimental profiles feature $W \leq 1$ in the outer region. This discrepancy arises from the different methods of scaling. In the numerical simulations we force $W = 1$ at the inflow boundary and $W_\infty \to 1$ is obtained at the side boundary for large X. The flow field ouside the wake region, thus, has velocity amplitudes $W > 1$ for reasons of continuity. In the experiments the velocity w_∞ for $x \to \infty$ is not accessible, since the channel has a finite width in both horizontal directions. Therefore, w_∞ is taken from the plateau of the measured profiles $w(x, z_i)$, which typically occurs in some outer region $|X| > 4$. By scaling with the averaged plateau value, all experimental profiles approach $W_\infty = 1$ outside the wake region. This discrepancy, therefore, is introduced artificially by the non-perfect scaling of the experimental data.

Secondly, the velocity defizit in the centre of the wake ($X = 0$) from the numerical simulation occurs smaller by about 12 % if compared to the experimental findings. This is likewise a consequence of the non-perfect experimental conditions. While the numerical and asymptotical results are obtained for a perfectly two-dimensional situation, the experimental results suffer to some degree from the presence of the walls. We, thus, have in the experiment a slight acceleration of the forced flow in the outer region and not

a perfectly-constant w_∞. These experimental imperfections are outlined in section 3.2 in some detail. In fact, three-dimensional numerical simulations have shown, that this discrepancy with respect to the wake amplitude is caused by the acceleration of the outer flow. While we have to be aware that the velocity amplitudes are not perfectly in accord, a careful analysis of the width of the wakes from both experimental measurements and numerical simulations proves excellent agreement.

The results for the vertical velocity profiles $W(X, Z_i)$ from the asymptotic model are collated in figure 5b. Following Schlichting (1982), we use a resistance coefficient of $c_w = 1.8$ for the Reynolds number $Re = 39.4$. We have compared our (numerically integrated) asymptotic results against the second-order expansion of Goldstein (1933), given likewise in Berger (1971). The profiles of both velocity components agree perfectly. Moreover, we find perfect agreement both with respect to the amplitude and the width of the wake between asymptotic model and experimental data. The asymptotic theory does not take into account the displacement effect of the cylinder as a solution for large z is inferred. This gives profiles with $W \leq 1$ outside the wake region. The loss of momentum due to the presence of the cylinder, on the other hand, is correctly reflected within the asymptotic model.

We find experimentally the power law

$$1 - W(0, Z) \propto Z^{-0.63} \tag{4.3}$$

for the wake amplitude. The corresponding asymptotic and numerical dependencies are

$$1 - W(0, Z) \propto Z^{-0.596}, \tag{4.4}$$

$$1 - W(0, Z) \propto Z^{-0.608}. \tag{4.5}$$

In all cases the power laws give an excellent representation of the data in the complete range $7.75 \leq Z \leq 17.75$. The width of the wake δ in the following is based on the criterion

$$\frac{1 - W(\delta, Z)}{1 - W(0, Z)} = \frac{1}{100}. \tag{4.6}$$

For the width δ we find experimentally no single power law dependency for the complete range in Z. On the other hand both asymptotic and numerical results are perfectly represented by the power laws

$$\delta \propto Z^{0.478}, \tag{4.7}$$

$$\delta \propto Z^{0.461}. \tag{4.8}$$

These power laws are obtained from least-square fits. The experimental data for $Z > 10.$, though, follow closely the above given theoretical dependencies.

4.2. *Weakly-heated cylinder*

In this section we shall give two typical results for flow fields featuring weak buoyant forces. The first example is obtained for a Grashof number of $Gr = 102.5$. Employing equation (2.86p) for the validity of the asymptotic model, we obtain for $Z_i = 7.75, 12.75, 17.75,$

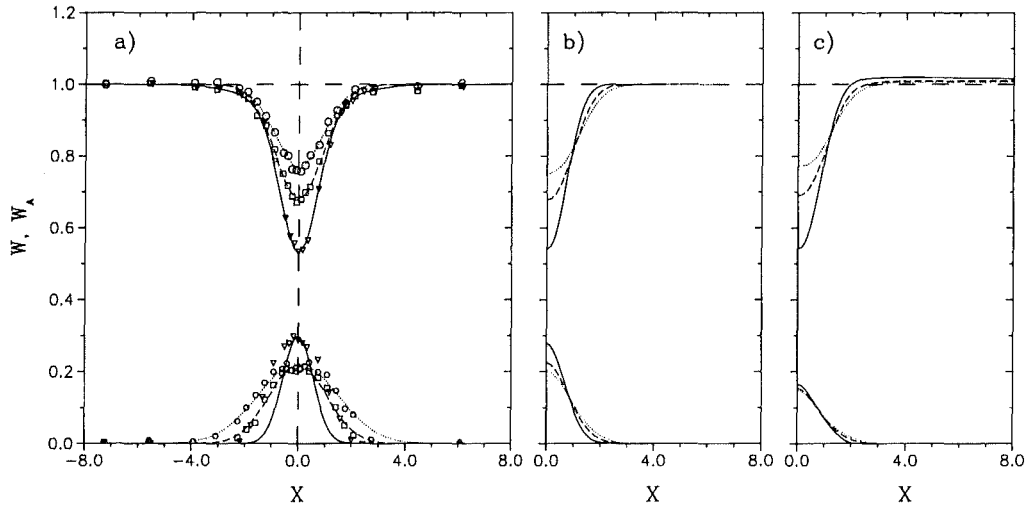

FIGURE 6. Profiles of the dimensionless vertical velocity $W(X, Z_i)$ and its buoyant contribution $W_A(X, Z_i)$ downstream of a weakly-heated cylinder. a) gives the experimental data and corresponding least-square fits, b) gives results from the asymptotic theory and c) gives results from the numerical simulations. The distances above the cylinder are $Z_i = 7.75, 12.75, 17.75$, the parameters are $Re = 39.4, \bar{c}_w = 1.3$, $Gr = 102.5, \Omega = 3.49, Pr = 6.13$.

$$\frac{\Omega Gr\sqrt{Z_i}}{Re^{5/2}} = 0.10, 0.13, 0.15 \ll 1. \tag{4.9}$$

Thus, we have ensured that the asymptotic model is valid for all Z_i. The results on the profiles $W(X, Z_i)$ are collated in figure 6. Even though the profiles look qualitatively similar in comparison to the forced flow profiles (cf. figure 5), an inspection of the amplitudes reveals, that buoyant forces have accelerated the flow in the wake centre. Given identical Reynolds numbers ($Re = 39.4$), the measured profiles for forced flow give values of $W(0, 7.75) \simeq 0.24$ on the centre line. For the weak buoyant flow ($Gr = 102.5$) we find, in contrast, $W(0, 7.75) \simeq 0.52$. The velocity deficit in the wake centre is, thus, reduced by a considerable amount due to buoyant foces.

In figure 6a the measured data from the experiment are plotted as symbols and least-square fits of the symmetric form

$$W(X, Z) = 1 - C_1 \exp(C_2 X^2) + C_3 \exp(C_4 X^2) \tag{4.10}$$

are given as solid lines. The last term in the form (4.10) is supposed to account for the buoyant contribution in the profiles. The form (4.10) allows for a reasonably-accurate fit to all experimental data and has been chosen based on the asymptotic results in equation (2.80p). In figure 6a in addition to the measured profiles $W(X, Z_i)$ the contribution from the buoyant forces

$$W_A(X, Z_i) = C_3 \exp(C_4 X^2) \tag{4.11}$$

is plotted. This is obtained experimentally from the difference between the actual profiles for $Gr = 102.5$ and the profiles for pure forced flow ($Gr = 0$). The experimental data in figure 6a suggest, firstly, wake-type profiles $W(X, Z_i)$, whereas the velocity defizit decreases downstream for increasing Z. Even though the data and fits indicate to some degree that the width of the wake increases downstream, a definitiv statement on this

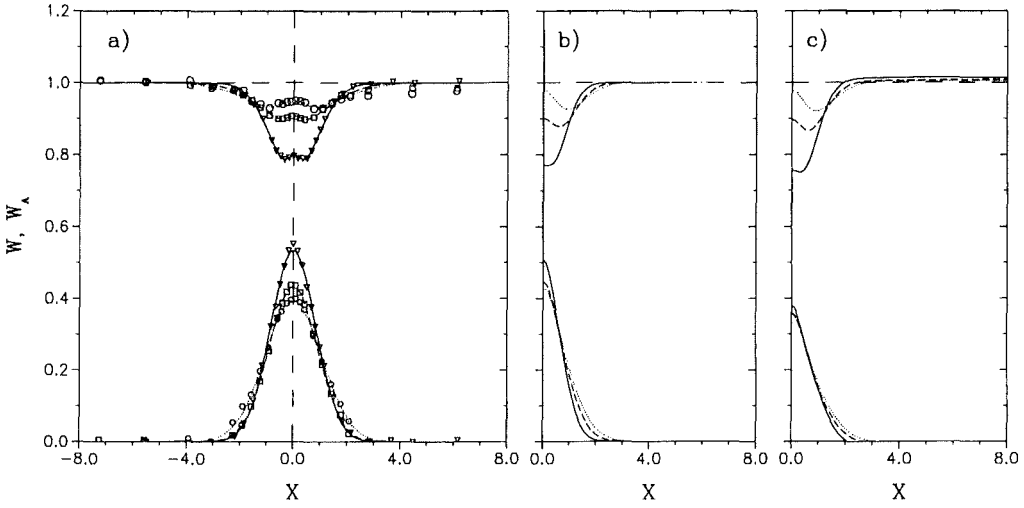

FIGURE 7. Profiles of the dimensionless vertical velocity $W(X, Z_i)$ and its buoyant contribution $W_A(X, Z_i)$ downstream of a weakly-heated cylinder. a) gives the experimental data and corresponding least-square fits, b) gives results from the asymptotic theory and c) gives results from the numerical simulations. The distances above the cylinder are $Z_i = 7.75, 12.75, 17.75$, the parameters are $Re = 39.4, \bar{c}_w = 1.0$, $Gr = 341.7, \Omega = 3.56, Pr = 6.13$.

question cannot be given due to slightly-scattered data. Secondly, the extracted profiles $W_A(X, Z_i)$ of the buoyant contribution have a narrow Gaussian shape at the first plane $Z_1 = 7.75$ (symbols $\bigtriangledown$) which develops downstream into a broader shape with smaller amplitudes.

The results from the asymptotic model occur in figure 6b. The overall profiles $W(X, Z_i)$ agree perfectly in both amplitude and width with the measured profiles at all locations Z_i (cf. figure 6a). From the asymptotic profiles a definite increase of the wake width downstream can be inferred. Inspecting the buoyant contribution $W_A(X, Z_i)$, we recognize the asymptotic results to perfectly resemble the experimental data from figure 6a. Again a Gaussian profile, which decreases in amplitude and develops a broader shape downstream is obtained. The numerical-simulation results in figure 6c, finally, agree well with both the experimental and the asymptotic results as far as the overall profiles $W(X, Z_i)$ are concerned. The buoyant contribution $W_A(X, Z_i)$, in contrast, exhibits in all planes Z_i smaller amplitudes. Moreover, the amplitudes of the buoyant contribution remain almost identical in all three planes Z_i. Here some discrepancy remains in comparison with both experimental and asymptotic findings, which both give decreasing amplitudes of the buoyant contribution downstream. This discrepancy is a direct consequence of the numerical forced-flow results (cf. figure 5c). Here the velocity defizit in the wake has been underpredicted, such that the difference between forced flow profiles and weak buoyant profiles gives likewise poor results.

Figure 7 relates to a somewhat higher temperature of the cylinder. In this case we have a Grashof number of $Gr = 341.7$ and can already infer from the velocity profiles $W(X, Z_i)$, that buoyant forces have led to a characteristic change. From relation (2.86p) we estimate the small parameter within the asymptotic model. We find in the three planes $Z_i = 7.75, 12.75, 17.75$

$$\frac{\Omega Gr\sqrt{Z_i}}{Re^{5/2}} = 0.35, 0.45, 0.53. \tag{4.12}$$

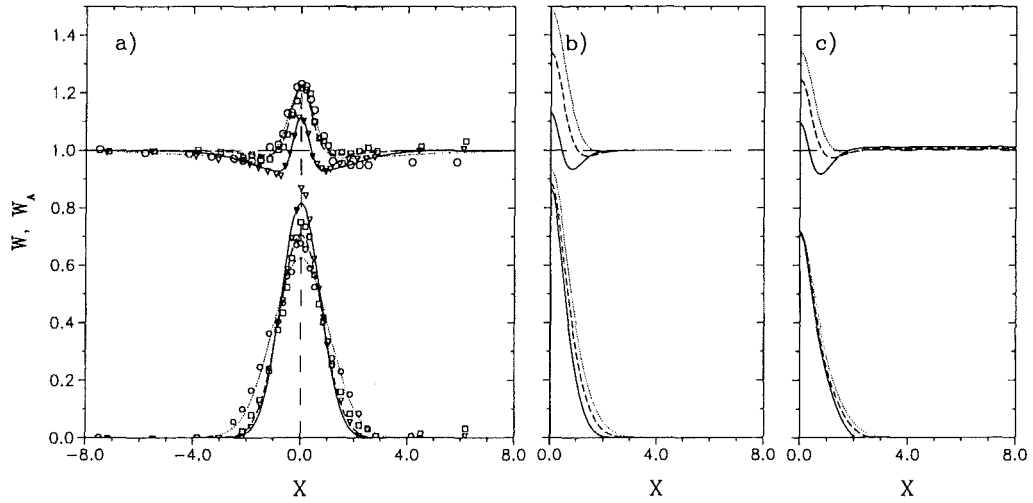

FIGURE 8. Profiles of the dimensionless vertical velocity $W(X, Z_i)$ and its buoyant contribution $W_A(X, Z_i)$ downstream of a strongly-heated cylinder. a) gives the experimental data and corresponding least-square fits, b) gives results from the asymptotic theory and c) gives results from the numerical simulations. The distances above the cylinder are $Z_i = 7.75, 12.75, 17.75$, the parameters are $Re = 39.4, \bar{c}_w = 0.9$, $Gr = 1025.1, \Omega = 3.89, Pr = 6.13$.

These numbers indicate that at least for large Z_i we are at the limit of the asymptotic model, as buoyant forces develop a substantial contribution to the flow field.

We continue to discuss the experimental findings, as collated in figure 7a. All measured velocity profiles $W(X, Z_i)$ indicate a pronounced buoyant acceleration of the fluid in the wake centre. The experimental observations are in good agreement with the corresponding asymptotic and numerical profiles $W(X, Z_i)$ (cf. figures 7b, 7c). This indicates that the asymptotic model remains perfectly valid even for this large Grashof number of $Gr = 341.7$. Aside of the velocity amplitudes, likewise the total width of the wake and the width of the inner buoyant zone are predicted correctly, both by the asymptotic model and the numerical simulation. If we focus onto the buoyant contribution $W_A(X, Z_i)$, we find in all profiles consistently a decrease of the amplitudes and an increase of the width of the buoyant zone downstream. The amplitudes of $W_A(X, Z_i)$ from the numerical simulation again have some discrepancies in comparison with the experimental amplitudes in figure 7a. The reason for this discrepancies is outlined above.

4.3. *Strongly-heated cylinder*

In figure 8 we have collated velocity profiles, obtained for a large Grashof number of $Gr = 1025.1$. For such a high cylinder temperature the hot fluid in the wake develops strong buoyant forces, comparable to inertial forces. This can be checked via relation (2.86p), which gives in the three planes $Z_i = 7.75, 12.75, 17.75$

$$\frac{\Omega Gr\sqrt{Z_i}}{Re^{5/2}} = 1.14, 1.46, 1.72. \tag{4.13}$$

Clearly, within this range of parameters the asymptotic model is not expected to be valid. Therefore, only a comparison of experimental and numerical (FEM) data occurs reasonable.

The experimental velocity profiles $W(X, Z_i)$ in figure 8a show only in the first plane $Z_1 = 7.75$ a discernible wake contribution (cf. symbols $\triangle$). The profiles further down-

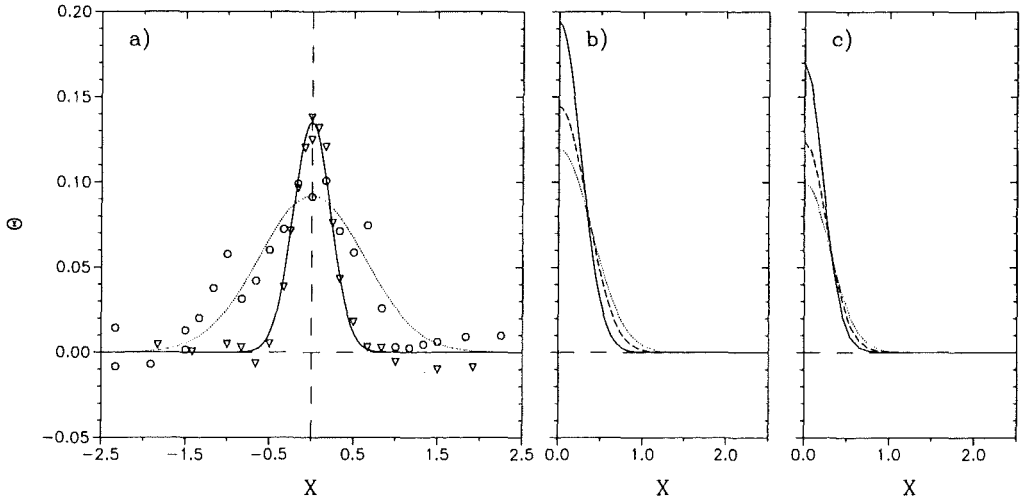

FIGURE 9. Profiles of the dimensionless temperature $\Theta(X, Z_i)$ downstream of a strongly-heated cylinder. a) gives the experimental data and corresponding least-square fits for Z_1, Z_3, b) gives results from the asymptotic theory and c) gives results from the numerical simulations. The distances above the cylinder are $Z_i = 7.75, 12.75, 17.75$, the parameters are $Re = 39.4, \bar{c}_w = 0.9$, $Gr = 1025.1, \Omega = 3.89$, $Pr = 6.13$.

stream ($Z_2 = 12.75, Z_3 = 17.75$) are dominated by a strong buoyant jet in the centre. An inspection of the buoyant contribution $W_A(X, Z_i)$ reveals, in accord with the weakly-heated cases, a narrow Gaussian profile with decreasing centre amplitude and increasing width downstream. The asymptotic model (cf. figure 8b) fails to predict these profiles at a reasonable accuracy. Firstly, the overall profiles $W(X, Z_i)$ exhibit far to high amplitudes in the centre. Secondly, the buoyant contribution $W_A(X, Z_i)$ in figure 8b shows even increasing amplitudes downstream. This is qualitatively in contradiction with the experimental findings in figure 8a. The widening of the Gaussian profile of $W_A(X, Z_i)$ from experiment and asymptotic model, though, happens to be in accord. To summarize, the asymptotic model for large Gr, outside its range of validity, overpredicts the buoyant effects.

The results from the corresponding numerical simulation are collated in figure 8c. The overall velocity profiles $W(X, Z_i)$ show a reasonable agreement with respect to the experimental data in figure 8a. The acceleration of the flow in the centre as one moves downstream, though, is slightly overpredicted by the numerical simulation. The buoyant contribution $W_A(X, Z_i)$ reveals a Gaussian profile of constant centre amplitude (in Z), which develops broader downstream. Once more, there remains a discrepancy with respect to the amplitude $W_A(0, Z_i)$: The experiment indicates a distinct decrease of the centre amplitude downstream.

As mentioned above, temperature profiles $\Theta(X, Z_i)$ have been measured in the experiments at much lower accuracy. This is due , firstly, to a temperature increase of always less than $0.2K$ in the first measuring plane and even smaller temperature amplitudes in the measuring planes downstream. Secondly, for high cylinder temperatures the situation is not perfectly stationary, leading to further errors from time-averaging. Nevertheless, it occurs useful to compare temperature profiles for the strongly-heated cylinder at least. The data are collated in figure 9. The experimental data occur in figure 9a for two planes, namely $Z_1 = 7.75, Z_3 = 17.75$, in form of the symbols $\circ$ and $\triangle$. Moreover, least-square fits of the form

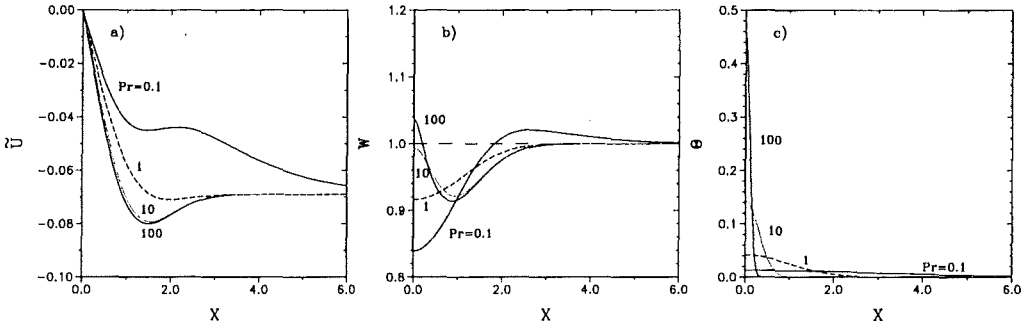

FIGURE 10. Profiles of a) the dimensionless horizontal velocity $\tilde{U}(X, Z_3)$, b) the dimensionless vertical velocity $W(X, Z_3)$, c) the dimensionless temperature $\Theta(X, Z_3)$ downstream of a weakly-heated body. The distance above the body is $Z_3 = 17.75$, the parameters are $Re = 39.4, \bar{c}_w = 1.0$, $Gr = 341.7, \Omega = 3.56$.

$$\Theta = C_1 \exp C_2 X^2 \tag{4.14}$$

are given by the solid and dotted lines. The profiles are of Gaussian type, whereas the peak temperature in the centre $\Theta(0, Z_i)$ decrease downstream and the width of the heated zone δ_{th} increases downstream. A qualitatively identical behaviour is obvious from the numerical simulation profiles in figure 9c. Quantitatively, however, the peak temperatures $\Theta(0, Z_i)$ from the numerical simulation are somewhat higher. Further, the widening of the heated zone δ_{th} downstream appears more pronounced in the experimental data. This discrepancy is presumably caused by slight temporal oscillations downstream of the cylinder in the experiment. This causes a more effective transport of momentum and heat in the horizontal direction X. Moreover, the time-averaging during the temperature measurements may lead to a smearing of the profiles.

Finally, the temperature profiles from the asymptotic model in figure 9b dramatically overestimate the peak temperature $\Theta(0, Z_i)$. Moreover, the width development is not in accord with the experimental data. This is not surprising, as equation (4.13) proves that we stress this model outside of its range of validity.

4.4. *Effect of Prandtl number*

At this stage we discuss the influence of various parameters onto the flow and temperature fields. In section 4.1-4.3 we have verified the asymptotic model against both experimental and numerical (FEM) findings. Thus, we carry this discussion purely on base of the asymptotic model, always obeying its range of validity (cf. section 2.4.3). Moreover, we restrict to the plane problem. One interesting parameter to discuss is the Prandtl number Pr. The Prandtl number characterizes the ratio of molecular transport of momentum and heat within the fluid and, thus, is a fluid property.

In figure 10 we collate a set of results, obtained for Prandtl numbers in the range $0.1 \leq Pr \leq 100$. The results are obtained for mixed-convective conditions and a weakly-heated body, i.e. the parameters are $Re = 39.4$, $Gr = 341.7$. The profiles are taken in a distance of $Z_3 = 17.75$ downstream of the body. From the temperature profiles $\Theta(X, Z_3)$ in figure 10c the influence of the Prandtl number is immediately obvious. For a large Prandtl number of $Pr = 100$ we have a poorly-conducting fluid, causing a narrow heated zone of thickness $\delta_{th} \simeq 0.3$. In contrast, a small Prandtl number of $Pr = 0.1$, due to good heat conduction in the fluid, leads to a wide heated zone of thickness $\delta_{th} \simeq 9$. The thickness of the heated zone, hereby, is defined by

$$\frac{\Theta(\delta_{th}, Z_i)}{\Theta(0, Z_i)} = \frac{1}{100}. \tag{4.15}$$

Similarly, the amplitude $\Theta(0, Z_3)$ of the Gaussian-type profiles is strongly dependent on the Prandtl number. Here we find an increase of the centre temperature $\Theta(0, Z_3)$ with increasing Prandtl number. A careful analysis of all data reveals that both the width of the heated zone δ_{th} and the centre temperature $\Theta(0, Z)$ follow a power law in the investigated range $5. \leq Z \leq 20$. For the complete range of Prandtl numbers $0.1 \leq Pr \leq 100$ we find the behaviour

$$\delta_{th} \propto Pr^{-0.504}, \tag{4.16}$$

$$\Theta(0, Z) \propto Pr^{0.523}. \tag{4.17}$$

The power law behaviour of both quantities can likewise be found from the leading-order term in equation (2.81p). The second-order term in equation (2.81p) does not change this behaviour significantly.

Depending on the temperature field, the buoyant forces will either be concentrated in the centre (cf. $Pr = 100$), or will be distributed over a wide range (cf. $Pr = 0.1$). The vertical velocity profiles $W(X, Z_3)$ in figure 10b reflect this, as for $Pr = 100$ only in a narrow centre zone the fluid is accelerated to velocities $W(0, Z_3) \geq 1$. For $Pr = 0.1$, in contrast, a wide range of fluid inside and outside of the wake experiences buoyant forces and, thus, only weak acceleration. For $Pr = 1$ we find the width of the heated zone δ_{th} and the width of the wake δ, defined by equation (4.6), to be equal, i.e. $\delta \simeq \delta_{th} \simeq 3$. The width of the wake δ remains independent of Prandtl number. The behaviour of the centre amplitude $W(0, Z)$ has likewise been analyzed with respect to a power law behaviour. Here, only in the limited range $0.1 \leq Pr \leq 10$ the data can be approximated by the power law

$$W(0, Z) \propto Pr^{0.032}. \tag{4.18}$$

For values $Pr > 10$ the amplitudes $W(0, Z)$ asymptotically approach a constant value for $Pr \to \infty$ in all planes Z_i. Physically this is expected, since even temperature profiles in form of a delta-function (for $Pr \to \infty$) due to viscous effects lead to buoyant jets of finite amplitude and width.

The horizontal velocity profiles $\tilde{U}(X, Z_3)$ in figure 10a in all cases show a transport of fluid from the far-outside region into the wake. The maximum amplitude of $\tilde{U}(X, Z_3)$ occurs for $Pr = 100$ at a position $X \simeq 1.5$. The curve for $Pr \to \infty$, in fact, cannot be distinguished from the curve obtained for $Pr = 100$. For smaller Prandtl numbers the amplitude of $\tilde{U}(X, Z_3)$ in the intermediate region decreases. The amplitude of $\tilde{U}(X \to \infty, Z_3)$ in the far-outside region, on the other hand, is not dependent on Pr.

4.5. *Effect of Grashof number*

The influence of the Grashof number, or in physical terms of the body temperature, is a further interesting parameter. We carry this discussion, once more, for the plane problem, based on the asymptotic model. Even though the above verification of the asymptotic model is performed for a heated body ($Gr \geq 0$), we extend the discussion to a cooled body ($Gr < 0$). In figure 11 a set of profiles, obtained for Grashof numbers in the range $-300 \leq Gr \leq 300$ is collated, whereas the Reynolds number is kept constant at $Re = 39.4$ and all profiles are taken in a distance $Z_3 = 17.75$ downstream of the body.

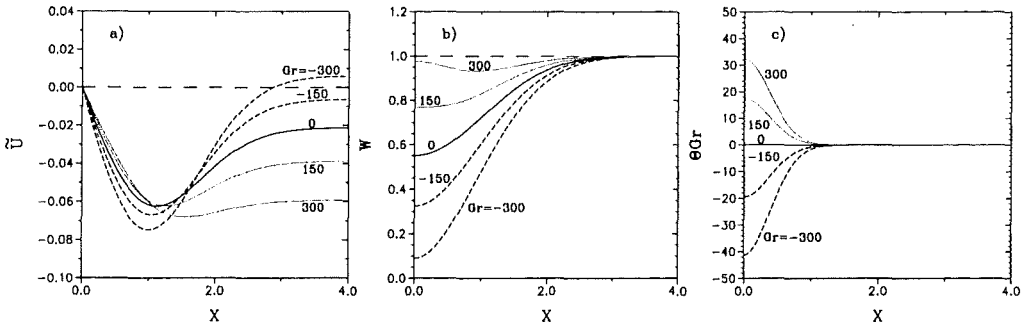

FIGURE 11. Profiles of a) the dimensionless horizontal velocity $\tilde{U}(X, Z_3)$, b) the dimensionless vertical velocity $W(X, Z_3)$, c) the dimensionless temperature $Gr\,\Theta(X, Z_3)$ downstream of a weakly-heated/weakly-cooled body. The distance above the body is $Z_3 = 17.75$, the parameters are $Re = 39.4$ and $Pr = 6.13$. The further parameters are approximated by $\Omega \simeq 3.5, \bar{c}_w \simeq 1.8 - 0.003Gr$.

Dimensionless profiles of the velocity components $\tilde{U}(X, Z_3)$ and $W(X, Z_3)$ are plotted in figures 11a,b and the sign-sensitive quantity $Gr\,\Theta(X, Z_3)$ occurs in figure 11c. The quantity $Gr\,\Theta$ is via

$$Gr\,\Theta(X, Z) = \frac{\alpha g d^3 (T - T_\infty)}{\nu^2} \tag{4.19}$$

directly proportional to the actual temperature $[T(X, Z) - T_\infty]$ of the fluid.

From the temperature profiles in figure 11c we recognize the expected Gaussian profiles across the wake and we find from the dotted profiles increasingly hot fluid in the wake centre for increasing Grashof numbers (cf. $Gr = 150, 300$). For $Gr = 0$ we recover the isothermal wake (solid profile). With decreasing Grashof numbers (cf. $Gr = -150, -300$) we have the body cooler than the ambient fluid and, thus, the dashed temperature profiles show cold fluid in the wake centre. Independent of the Grashof number, the heated/cooled zone is of thickness $\delta_{th} \simeq 1$. The centre amplitude $Gr\,\Theta(0, Z_3)$ is found to behave like

$$Gr\,\Theta(0, Z_3) \propto Gr^{0.967}, \tag{4.20}$$

which indicates that $\Theta(X, Z)$, following equation (2.81p), does not develop a dependency on Gr. The form function $H(\eta)$ in equation (2.81p) remains independent of Gr.

The kinematic effect of the hot/cold fluid in the wake onto the vertical velocity $W(X, Z_3)$ can be inspected in figure 11b. Here we find an acceleration of the hot fluid in the wake centre from the dotted profiles (cf. $Gr = 150, 300$) if compared to the isothermal wake ($Gr = 0$). This effect has already been discussed in sections 4.2 and 4.3. Cold fluid in the wake, in contrast, is retarded due to its higher specific weight. This can be inferred from the dashed profiles obtained for the cooled body (cf. $Gr = -150, -300$), which show an increasingly strong velocity deficit in the wake centre. Thus, cold fluid has a similar effect as an increase of the drag coefficient, as both lead to more pronounced wake profiles. The centre amplitude $W(0, Z_3)$ of the vertical velocity almost exactly follows the proportionality

$$W(0, Z_3) \propto Gr^{1.0}. \tag{4.21}$$

As both form functions $F(\eta), K(\eta)$ in equation (2.80p) are independent of Gr, this behaviour is in agreement with the explicit linear dependency in equation (2.80p).

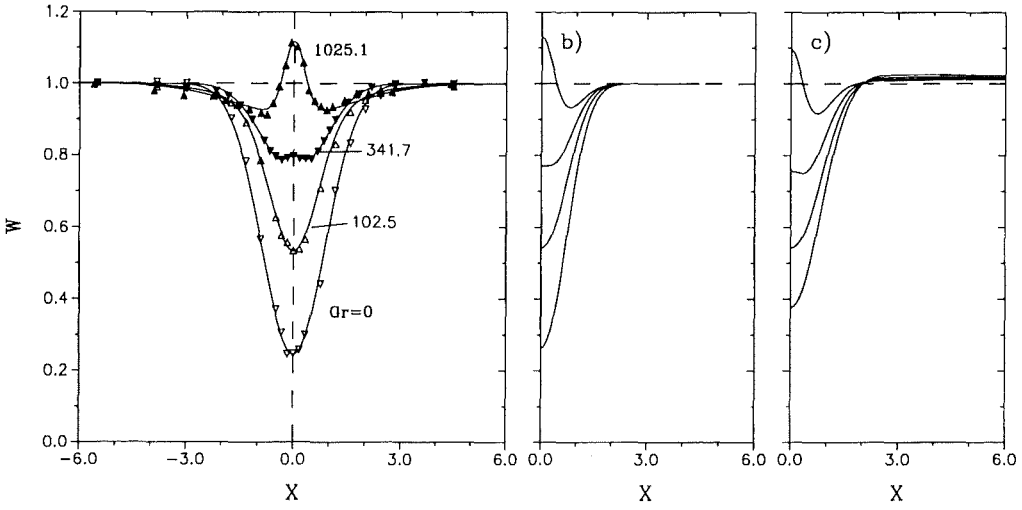

FIGURE 12. Profiles of the dimensionless vertical velocity $W(X, Z_1)$ downstream of the cylinder for various temperatures T_b. a) gives the experimental data and corresponding least-square fits, b) gives results from the asymptotic theory and c) gives results from the numerical simulations. The distance above the cylinder is $Z_1 = 7.75$, the parameters are $Re = 39.4$, $Pr = 6.13$, $Gr = 0, 102.5, 341.7, 1025.1$.

The profiles of the horizontal velocity component $\tilde{U}(X, Z_3)$ are given in figure 11a. For the isothermal body (cf. $Gr = 0$) the solid profile indicates a flow of ambient fluid into the wake centre ($\tilde{U} < 0$), which persists for $X \to \infty$. The heated body (cf. $Gr = 150, 300$) clearly intensifies the inward flow, as the dotted profiles show larger amplitudes for $X \to \infty$. This is a consequence of the vertical acceleration of the hot fluid in the wake centre, which in turn demands a higher supply of fluid from the ambient. If the body is cooled (cf. $Gr = -150, -300$) the situation develops quite differently. Now the vertical retardation of the cold fluid in the wake centre may lead even to a horizontal flow outward into the ambient ($U > 0$), as obvious from the dashed profiles. The amplitude $\tilde{U}(X \to \infty, Z_3)$ of the horizontal velocity far outside follows the law

$$\tilde{U}(X \to \infty, Z_3) \propto Gr^{1.04}. \tag{4.22}$$

The almost identical power laws in equations (4.21,4.22) prove the consistency of these results, asd independent of Gr conservation of mass (cf. equation (2.13)) is preserved. The last term in equation (2.79p) is responsible for the behaviour $\eta \to \infty$. Both form functions $G(\eta), I(\eta)$ do not have a dependency on Gr. Thus, in all cases (2.79p-2.81p) the dependencies on Gr are explicitely known.

The above statements concerning the influence of the Grashof number Gr onto the flow field can be verified by the experimental measurements and by the numerical simulations of the vertical velocity profiles $W(X, Z_i)$. A comparison of these profiles in the plane $Z_1 = 7.75$ is conducted in figure 12. We recognize a reasonably good agreement of the profiles obtained by all three methods. The agreement holds for all Grashof numbers, whereas slight discrepancies occur for the case of the strongly-heated cylinder with $Gr = 1025.1$. Here the asymptotic model is stressed outside its range of validity. A further experimental verification can be obtained from a comparison of the measured centre amplitudes $W(0, Z_3)$ in the plane $Z_3 = 17.75$ and the power law (4.21), found from the asymptotic model. We exclude the data for $Gr = 1025.1$ and find from the experimental data the least-square fit

$$W(0, Z_3) \simeq 0.581 + 1.126 \cdot 10^{-2}\, Gr^1. \tag{4.23}$$

Thus, the experimental data at good accuracy confirm the linear law in the range of moderate Grashof numbers.

5. Conclusion

We have studied the flow and temperature fields in wakes above heated bodies. The problem is either plane for infinitely long horizontal cylindrical bodies or axisymmetric for spherical bodies. In all cases we consider the laminar flow of a Newtonian fluid, subject to inertial forces, viscous forces and buoyant forces. Buoyant forces are modelled by invoking the Boussinesq approximation. This mixed-convection problem is characterized by three dimensionless groups, namely the Reynolds number, the Grashof number and the Prandtl number.

We use three principal means of investigation. (a) In the body of this article an asymptotic model for the problem is developed, which, based on boundary layer theory, is valid for large Reynolds numbers and large Péclet numbers $Pe = RePr$. Further expansions restrict to the far wake and to weak buoyant forces. Within the framework of the asymptotic model the buoyant effects occur essentially as a linear superposition to the forced flow. This model allows to deduce analytical expressions in selfsimilar form for the flow and temperature fields in both plane and axisymmetric geometry. The analytical expressions explicitely give most of the parameter dependencies, while a system of ordinary differential equations for the shape functions is left for numerical integration. Only the thermal shape functions exhibit a dependency on the Prandtl number. To validate the asymtotic model, experiments and FEM simulations in a plane geometry are employed. (b) The experiments are performed in a vertical water channel ($Pr \simeq 6$), where a horizontal isothermal cylinder of $6mm$ diameter is positioned. Both, profiles of the vertical velocity and profiles of the temperature are measured in distances $7.75 \leq z/d \leq 17.75$ above the cylinder by means of Laser Doppler Anemometry and thermocouples. The parameter range in the experiments is $Re \simeq 40$, $0 \leq Gr \leq 1025$. (c) The FEM simulations use a commercial code (FIDAP 7.6) to compute the flow and temperature fields on a mesh of about 25,000 nodes. The computational domain extends horizontally from the symmetry line sufficiently outward, i.e. $0 \leq x/d \leq 30$. Vertically it extends sufficiently far into both upstream and downstream direction and cover the range $-50 \leq z/d \leq 60$.

We find in the heated wake above the cylinder buoyant forces leading to an acceleration of the flow and, thus, to a faster reduction of the velocity deficit in the wake centre. For strong heating this acceleration may even lead to vertical velocity amplitudes larger than the forced flow amplitude, particularly in the wake centre. The amplitude of the buoyant contribution in the vertical velocity profile increases with increasing Grashof number. To be precise, the buoyant forces are governed by the group Gr/Re^2. In conjunction with the vertical movement of fluid, a horizontal transport of fluid from far outside into the wake centre is characteristic for the isothermal wake. This horizontal transport is also modified by buoyant forces. For the heated wake strong buoyant forces demand a more intense horizontal transport of fluid into the wake centre. Therefore, the horizontal velocity far outside the wake increases likewise with increasing Grashof number. For a cooled wake, instead, a retardation of the fluid in the wake centre is present. This reduces the horizontal flow into the wake centre and may even cause a horizontal flow outward from the wake centre into the ambient.

The Prantdl number governs the width of the thermal wake, which in general is different from the width of the kinematic wake. Small Prandtl numbers result in a wide thermal wake causing buoyant forces across the complete kinematic wake and outside therefrom. Thus, as heat is distributed over a wide range, the local temperature rise and the resulting buoyant force appear relatively weak. In contrast, large Prandtl numbers are responsible for narrow thermal wakes, liberating buoyant forces in a narrow subregion of the kinematic wake. Thus, a slender buoyant jet in the wake centre with relatively strong acceleration develops.

The asymptotic model has been validated against both experiments and FEM simulations. This implies that for plane geometry the model predictions compare well with the results obtained from experimens and numerics and the range of validity is carefully evaluated. As the model is likewise developed for axisymmetric geometry, an experimental or numerical validation of this aspect occurs worthwhile. There are further possibilities to extend the model. Of course, the laminar assumption restricts to a limited parameter range and, therefore, does not permit to apply the model to technical apparatuses as e.g. heat exchangers. An extension of the present model towards turbulent flow, therefore, occurs highly attractive. In fact, the Reynolds-averaged conservation equations could serve as basis for the development of an analogous turbulent model. After the boundary layer approximation, the far-wake expansion and the assumption of weak buoyant forces are applied, these equations for the time-averaged velocities and temperature are almost identical with the laminar set of equations. However, we would have a turbulent shear stress and a turbulent heat flux present as opposed to the diffusive terms in the laminar set of equations. Here reasonable closure conditions would be required. Thus, the laminar model may deliver the scheme for the treatment of the turbulent problem under similar assumptions and approximations.

I like to thank my students F. Fellmoser, R. Griesbaum, V. Sarnes and A. Wintruff, who all contributed to this work while elaborating their Diploma thesis at the University of Karlsruhe, respectively the Engineering College of Karlsruhe. Moreover, I would like to acknowledge the contribution of my student U. Siegel from the Engineering College of Offenburg, who engaged himself in the comparing computations and plots during the preparation of this manuscript.

REFERENCES

AFZAL, N. 1981 Mixed convection in a two-dimensional buoyant plume. *J. Fluid Mech.* **105**, 347-368.

AFZAL, N. 1983 Mixed convection in an axisymmetric buoyant plume. *Int. J. Heat Mass Transfer* **26**, 381-388.

AFZAL, N. 1985 Mixed convection plume above a point heat source in a vertical free stream. *Int. J. Heat Mass Transfer* **28**, 2043-2047.

BERGER, S.A. 1968 The incompressible laminar axisymmetric far wake. *J. Mathematics and Physics* **47**, 292-309.

BERGER, S.A. 1971 Laminar wakes. Elsevier Publ., New York.

BETCHOV, R.& CRIMINALE, W.O. 1967 Stability of parallel flows. Academic Press, New York.

BRAND, R.S. & LAHEY, F.J. 1967 Heated laminar vertical jet. *J. Fluid Mech.* **29**, 305-315.

BRODOWICZ, K. & KIERKUS, W.T. 1966 Experimental investigation of laminar free convection flow in air above horizontal wire with constant heat flux. *Int. J. Heat Mass Transfer* **9**, 81-94.

CHURCHILL, S.W.& CHU, H.H.S. 1975 Correlating equations for laminar and turbulent free convection from a horizontal cylinder. *Int. J. Heat Mass Transfer* **18**, 1049-1053.

COLLIS, D.C. & WILLIAMS, M.J. 1959 Two-dimensional convection from heated wire at low Reynolds numbers. *J. Fluid Mech.* **6**, 357-384.

CRANE, L.J. 1975 Axially symmetric plumes at very small Prandtl numbers. *J. Appl. Mathematics and Physics* **26**, 427-435.

FORSTROM, R.J. & SPARROW, E.M. 1967 Experiments on the buoyant plume above a heated horizontal wire. *Int. J. Heat Mass Transfer* **10**, 321-331.

FUJII, T. 1963 Theory of the steady laminar natural convection above a horizontal line heat source and a point heat source. *Int. J. Heat Mass Transfer* **6**, 597-606.

FUJII, T., MORIOKA, I., UEHARA, H. 1973 Buoyant plume above a horizontal line heat source. *Int. J. Heat Mass Transfer* **16**, 755-768.

GEBHART, B. & PERA, L. 1970 Mixed convection from long horizontal cylinders. *J. Fluid Mech.* **45**, 49-64.

GEBHART, B., PERA, L., SCHORR, A.W. 1970 Steady laminar natural convection plumes above a horizontal line source. *Int. J. Heat Mass Transfer* **13**, 161-171.

GEBHART, B., JALURIA, Y., MAHAJAN, R.L., SAMMAKIA, B. 1988 Buoyancy-induced flow and transport. Hemisphere Publ., Washington.

GNIELINSKI, V. 1975 Berechnung mittlerer Wärme- und Stoffübergangskoeffizienten an laminar und turbulent überströmten Einzelkörpern mit Hilfe einer einheitlichen Gleichung. *Forsch.-Ing. Wesen* **41**, Nr.5, 145-153.

GOLDSTEIN, S. 1933 On the two-dimensional steady flow of a viscous fluid behind a solid body. *Proc. Roy. Soc. (London)* **A142**, 545-562.

HATTON, A.P., JAMES, D.D., SWIRE, H.W. 1970 Combined forced and natural convection with low-speed air flow over horizontal cylinders. *J. Fluid Mech.* **42**, 17-31.

HIEBER, C.A. & GEBHART, B. 1969 Mixed convection from a sphere at small Reynolds and Grashof numbers. *J. Fluid Mech.* **38**, 137-159.

KUIKEN, H.K. & ROTEM, Z. 1971 Asymptotic solution for plume at very large and small Prandtl numbers. *J. Fluid Mech.* **45**, 585-600.

LIÑÁN, A. & KURDYUMOV, V.N. 1998 Laminar free convection induced by a line heat source, and heat transfer from wires at small Grashof numbers. *J. Fluid Mech.* **362**, 199-227.

LOITSIANSKI, L.G. 1967 Laminare Grenzschichten. Akademie-Verlag, Berlin.

LUGT, H.J. 1979 Wirbelströmung in Natur und Technik. Verlag G. Braun, Karlsruhe.

RILEY, D.S. & DRAKE, D.G. 1983 Mixed convection in an axisymmetric buoyant plume. *Q. J. Mech. appl. Maths.* **36**, 43-54.

ROUSE, H., YIH, C.S., HUMPHREYS, H.W. 1952 Gravitational convection from a boundary source. *Tellus* **4**, 201-210.

SCHLICHTING, H. 1982 Grenzschicht-Theorie. Verlag G. Braun, Karlsruhe.

SCHUH, H. 1948 Boundary layers of temperature. In *Boundary Layers,* by W. Tollmien. British Ministry of Supply, German Document Centre, Reference 3220T.

SPALDING, D.B. & CRUDDACE, R.G. 1961 Theory of the steady laminar buoyant flow above a line heat source in a fluid of large Prandtl number and temperature-dependent viscosity. *Int. J. Heat Mass Transfer* **3**, 55-59.

STEWARTSON, K. 1957 On asymptotic expansions in the theory of boundary layers., *J. Mathematical Physics* **36**, 173-191.

TOLLMIEN, W. 1931 Grenzschichttheorie. In *Handbuch der Experimentalphysik Bd. IV*, 242-287. Akademie-Verlag, Leipzig.

WESSELING, P. 1975 An asymptotic solution for slightly buoyant laminar plumes. *J. Fluid Mech.* **70**, 81-87.

WOOD, W.W. 1972 Free and forced convection from fine hot wires. *J. Fluid Mech.* **55**, 419-438.

YIH, C.-S. 1951 Free convection due to a point source of heat. *Proc. 1st U.S. Natn. Congr. Appl. Mech.*, 941-947.

YIH, C.-S. 1952 Laminar free convection due to a line source of heat. *Trans. Am. Geophys. Union* **33**, 669-672.

ZELDOVICH, YA.B. 1937 The asymptotic laws of freely-ascending convective flows. *Zh. Eksp. Teor. Fiz.* **7**, 1463-1465.

ŽUKAUSKA, A. & ŽIUGŽDA, J. 1985 Heat transfer of a cylinder in crossflow. In *Experimental and applied heat transfer guide books* (ed. G.F. Hewitt). Hemisphere Publ., Washington.